Natural break-up and satellite formation regimes of surfactant-laden liquid threads

A. Martínez-Calvo[1]†, J. Rivero-Rodríguez[2], B. Scheid[2], and A. Sevilla[1]

[1]Grupo de Mecánica de Fluidos, Departamento de Ingeniería Térmica y de Fluidos, Universidad Carlos III de Madrid, Av. Universidad 30, 28911 Leganés (Madrid), Spain

[2]TIPs, Université Libre de Bruxelles, C.P. 165/67, Avenue F. D. Roosevelt 50, 1050 Bruxelles, Belgium

(Received xx; revised xx; accepted xx)

We report a numerical analysis of the unforced break-up of free cylindrical threads of viscous Newtonian liquid whose interface is coated with insoluble surfactants, focusing on the formation of satellite droplets. The initial conditions are harmonic disturbances of the cylindrical shape with a small amplitude ϵ, and whose wavelength is the most unstable one deduced from linear stability theory. We demonstrate that, in the limit $\epsilon \to 0$, the problem depends on two dimensionless parameters, namely the Laplace number, $La = \rho\sigma_0\bar{R}/\mu^2$, and the elasticity parameter, $\beta = E/\sigma_0$, where ρ, μ and σ_0 are the liquid density, viscosity and initial surface tension, respectively, E is the Gibbs elasticity and $\bar{R}$ is the unperturbed thread radius. A parametric study is presented to quantify the influence of La and β on two key quantities: the satellite droplet volume and the mass of surfactant trapped at the satellite's surface just prior to pinch-off, V_{sat} and Σ_{sat}, respectively. We identify a weak-elasticity regime, $\beta \lesssim 0.125$, in which the satellite volume and the associated mass of surfactant obey the scaling law $V_{sat} = \Sigma_{sat} = 0.0042La^{1.64}$ for $0.05 \lesssim La \lesssim 2$, while V_{sat} and Σ_{sat} become negligible when $La \lesssim 0.05$. For $La \gtrsim 10$, V_{sat} and Σ_{sat} reach a plateau of about 3% and 2.9% respectively, V_{sat} being in close agreement with previous experiments of low viscosity threads with clean interfaces. For $La < 7.5$, we reveal the existence of a discontinuous transition at a critical elasticity, $\beta_c(La)$, with $\beta_c \to 0.98$ for $La \lesssim 0.2$, such that no satellite droplet is formed when $\beta < \beta_c$, while a satellite droplet with finite volume and finite surfactant mass appears for $\beta > \beta_c$.

Key words: Capillary flows, Instability, Surfactants

1. Introduction

The breakup of free-surface flows has been investigated for a long time. The first quantitative studies on the instability responsible for the spontaneous breakup of cylindrical liquid threads date back to the 19th century; the correct physical description of the instability mechanism was due to Plateau (1873), who deduced that a small perturbation with a wavelength larger than the circumference of the unperturbed column is unstable, finally breaking up into main drops and smaller satellite droplets in between. A few years later, Rayleigh (1878, 1892) calculated the most unstable wavelength using a linear

† Email address for correspondence: amcalvo@ing.uc3m.es

temporal stability analysis. The subject experienced a renaissance fifty years ago that lasts to date due to its central role in industrial and medical applications such as chemical reactors, ink-jet and 3D printing, additive manufacturing, drug and protein encapsulation or cytometry, to cite a few (the reader is referred to the reviews of Bogy 1979; Eggers 1997; Christopher & Anna 2007; Eggers & Villermaux 2008; Derby 2010; Anna 2016).

The theoretical approach to study the dynamics of jet breakup was first based on the linear stability analysis of infinite liquid threads. As already mentioned, the local temporal approach was pioneered by Rayleigh (1892). About eighty years later, the local spatial and spatiotemporal problems, in which the liquid jet moves with uniform velocity U with respect to the injector, were solved (Keller *et al.* 1973; Leib & Goldstein 1986*a*,*b*). In particular, it was demonstrated by Keller *et al.* (1973) that the spatial and temporal stability analyses are equivalent if U is sufficiently larger than the speed of small-amplitude capillary instability waves, U_σ. In the spatial setting, the latter condition means that the relative growth of the wave amplitude along one wavelength is small. Thus, in a frame of reference moving with the jet, the amplitude growth is spatially uniform in a first approximation, what explains the equivalence of the temporal and spatial approaches if $U \gg U_\sigma$. Since the wavelength of the unstable capillary waves is much larger than the unperturbed cylinder radius, $\bar{R}$, the scaling of U_σ depends on the value of the associated Reynolds number, $Re_\sigma = \rho U_\sigma \bar{R}/\mu$, where ρ and μ are the liquid density and viscosity, respectively. In the limit of Euler flow, $Re_\sigma \gg 1$, the value of U_σ is given by the balance $\sigma_0/\bar{R} \sim \rho U_\sigma^2$, where σ_0 is the surface tension, yielding $U_\sigma \sim \sqrt{\sigma_0/(\rho\bar{R})}$, usually referred to as the *capillary velocity*, and $U/U_\sigma \sim \sqrt{We}$, where $We = \rho U^2 \bar{R}/\sigma_0$ is the Weber number. Note that, in this case, $Re_\sigma = \sqrt{La} \gg 1$, where $La = \rho\bar{R}\sigma_0/\mu^2$ is the Laplace number, which may also be written as $La = Oh^{-2}$ in terms of the usual Ohnesorge number, $Oh = \mu/\sqrt{\rho\bar{R}\sigma_0}$. In the opposite limit of Stokes flow, $Re_\sigma \ll 1$, the proper balance is $\sigma_0/\bar{R} \sim \mu U_\sigma/\bar{R}$, whence $U_\sigma \sim \sigma_0/\mu$, usually referred to as the *visco–capillary velocity*. In this limit, $U/U_\sigma \sim Ca$, where $Ca = \mu U/\sigma_0$ is the capillary number, and $Re_\sigma = La \ll 1$. Therefore, the condition that must be satisfied for the temporal and spatial approaches to be equivalent is that $\sqrt{We} \gg 1$ when $\sqrt{La} \gg 1$, or that $Ca \gg 1$ when $La \ll 1$. It is also important to point out that the formation of a slender jet from a nozzle requires that $We > We_c \sim O(1)$ when $\sqrt{La} \gg 1$, or that $Ca > Ca_c \sim O(1)$ when $La \ll 1$, where We_c and Ca_c are the critical Weber and capillary numbers for the transition from convective to absolute instability (Leib & Goldstein 1986*a*,*b*).

Many experimental studies have been carried out, from the first investigations of Savart (1833), Magnus (1859), Plateau (1873), Rayleigh (1882), and Donnelly & Glaberson (1966), to the highly-accurate measurements of González & García (2009), whose aim was to describe the mechanism of instability and to measure the growth rate of the associated waves in the linear regime. These experiments have shown an excellent agreement with the dispersion relation obtained by Rayleigh (Rayleigh 1878, 1892) and by Chandrasekhar (1961). It is important to emphasise that, although linear stability theory cannot describe the final stages of the dynamics prior to pinch-off, it can be used to predict the break-up time $\bar{t}_b$ with small relative errors, provided that the initial amplitude of the disturbance, ε, accomplishes $\epsilon = \varepsilon/\bar{R} \ll 1$. In the spatial setting, this fact can be used to estimate the break-up length as $U\bar{t}_b$, in close agreement with the experiments (Kalaaji *et al.* 2003; González & García 2009).

However, to describe the satellite formation process, which is the main objective of the present study, a nonlinear approach is needed. In particular, Goedde & Yuen (1970) first investigated such nonlinear effects in detail, comparing their experiments with the weakly nonlinear theory of Yuen (1968). The satellite drop formation process was first quantified by Rutland & Jameson (1970) and Lafrance (1975), while Chaudhary & Maxworthy

(1980) studied how the satellite drop formation is affected by forcing the liquid jet with different harmonics, revealing the conditions needed to inhibit their formation. These efforts to control drop formation were mainly motivated by the practical need of increasing the performance of the inkjet printing devices under development at that time. The increase in computational power finally allowed a fully nonlinear approach by means of direct numerical simulations of the axisymmetric Navier-Stokes equations. In particular Mansour & Lundgren (1990) and Ashgriz & Mashayek (1995) computed the satellite droplet radii just prior to pinch-off, finding an excellent agreement with the experiments of Rutland & Jameson (1970) and Lafrance (1975). Due to the high numerical cost of accurately solving the Navier-Stokes equations with a free boundary up to times close to the break-up singularity, several works have been devoted to develop one-dimensional approximations by expanding the flow variables as powers of the radial coordinate (see e.g. Lee 1974; Eggers & Dupont 1994; García & Castellanos 1994). These models have been proved to work reasonably well in different configurations (see e.g. Ambravaneswaran *et al.* 2004; Rubio-Rubio *et al.* 2013; Martínez-Calvo *et al.* 2018). Of particular importance is the fact that the leading-order model allowed to unravel the universal self-similar structure of the local flow close to the singularity (Eggers 1993; Papageorgiou 1995).

The presence of surfactant molecules at the interface induces an effective surface rheology by means of Marangoni stresses and surface viscosities (for a review, see Langevin 2014), leading to substantial changes in the dynamics with respect to the case of clean interfaces. Indeed, different flow configurations of technological interest are affected by surfactants, for instance liquid bridges (Liao *et al.* 2006), dip coating (Scheid *et al.* 2010; Delacotte *et al.* 2012; Champougny *et al.* 2015), or drop breakup (Roché *et al.* 2009; Ponce-Torres *et al.* 2017; Kamat *et al.* 2018), to cite a few. Regarding liquid threads, the effect of surfactants has been explored by means of theory (Timmermans & Lister 2002; Martínez-Calvo & Sevilla 2018) and numerical simulations (Campana & Saita 2006; Dravid *et al.* 2006; McGough & Basaran 2006; Kamat *et al.* 2018). In particular, the two latter works are focused on the micro-thread cascade that appears close to break-up due to the presence of surfactants. These works also analyse the different scalings close to pinch-off and the evolution of the minimum radius of the thread and its axial position during the unfolding of the micro-cascade. In contrast, the present work aims at providing a global parametric description of the satellite drop formation process when the interface is coated with an insoluble surfactant monolayer.

Given the success of the leading-order one-dimensional approximation in capturing the nonlinear dynamics of clean interfaces (Eggers & Dupont 1994; Subramani *et al.* 2006; Yildirim *et al.* 2005; Rubio-Rubio *et al.* 2013), similar models have been derived that account for the presence of surfactants, and numerically solved in different flow configurations (Ambravaneswaran & Basaran 1999; Craster *et al.* 2002, 2009; Xu *et al.* 2007). However, as pointed out by Timmermans & Lister (2002) and Martínez-Calvo & Sevilla (2018), a higher-order approximation is needed when the surface viscoelastic stresses are large enough. Therefore, following a similar strategy as Ashgriz & Mashayek (1995) and Dravid *et al.* (2006) for a clean and a surfactant-laden interface, respectively, in the present contribution our approach is to numerically integrate the Navier-Stokes equations in a temporal setting. Unlike Dravid *et al.* (2006), we use a nonlinear equation of state to relate the surface tension with the surfactant concentration, derived from first principles, that leads to substantial differences calling out for a careful experimental analysis. Moreover, we perform an exhaustive parametric study, accurately quantifying the volume of the satellite droplet prior to pinch-off and the amount of surfactant trapped

at its surface, as a function of the two dimensionless governing parameters, namely the elasticity parameter and the Laplace number.

The remainder of the paper is organised as follows: in §2 we describe the mathematical model and the numerical method employed for the simulations. In §3 we first validate the simulations by comparing the initial growth rate of small harmonic disturbances with the results provided by a temporal stability analysis. We then unravel the structure of the parameter plane spanned by the Laplace and elasticity numbers in terms of the satellite formation process, followed by a detailed analysis of the volume of the satellite droplets and their shape at break-up, the mass of surfactant trapped at their surface, and the nonlinear correction to the linear break-up time. The detailed time evolution is studied in several representative cases to provide physical explanations of the results obtained. Conclusions are drawn in §4.

2. Mathematical model and numerical method

We consider an infinite axisymmetric liquid thread of density ρ, viscosity μ, surface tension $\bar{\sigma}$ and unperturbed radius $\bar{R}$, which occupies a volume $\mathcal{V}(\bar{t})$ and is embedded in a passive ambient at constant pressure p_a in the absence of gravity. The interface $\partial\mathcal{V}(\bar{t})$, placed at a radial position $\bar{r} = \bar{a}(\bar{z}, \bar{t})$, is coated with a superficial concentration $\bar{\Gamma}$ of insoluble surfactant molecules (see figure 1a). Note that $\bar{r}$, $\bar{z}$ and $\bar{t}$ stand for the radial and axial coordinates and time, respectively. Henceforth the upper bar will denote dimensional variables if not specified otherwise. The effect of the adsorbed surfactant at the interface is to reduce the effective surface tension by an amount that depends on $\bar{\Gamma}$, and thus any disturbance of the interface shape generates an imbalance in $\bar{\Gamma}$ that produces a surface stress due to gradients of $\bar{\sigma}(\bar{\Gamma})$. For simplicity, in the present work we assume that surface viscous stresses can be neglected, thus disregarding the role of the surface shear and dilatational viscosities, μ_s and κ_s, respectively. The latter approximation is accurate provided that the corresponding Boussinesq numbers are small, namely $\mathscr{B}_\mu = \mu_s/(\mu\bar{R}) \ll 1$ and $\mathscr{B}_\kappa = \kappa_s/(\mu\bar{R}) \ll 1$ (Martínez-Calvo & Sevilla 2018). The problem is nondimensionalised with the viscocapillary time, $\mu\bar{R}/\sigma_0$, as characteristic time and with $\bar{R}$ as characteristic length, σ_0 being the surface tension associated to the initial concentration of insoluble surfactant at the interface $\bar{\Gamma}(\bar{z}, 0) = \Gamma_0$, which are used to scale the surface tension and the surface concentration, respectively.

The flow is governed by the dimensionless Navier-Stokes equations,

$$\boldsymbol{\nabla}\cdot\boldsymbol{u} = 0 \qquad \text{at } \mathcal{V}, \tag{2.1}$$

$$La\left(\frac{\partial \boldsymbol{u}}{\partial t} + \boldsymbol{u}\cdot\boldsymbol{\nabla}\boldsymbol{u}\right) = \boldsymbol{\nabla}\cdot\boldsymbol{T} \qquad \text{at } \mathcal{V}, \tag{2.2}$$

where $\boldsymbol{u}(\boldsymbol{x}, t) = u\,\boldsymbol{e}_r + w\,\boldsymbol{e}_z$ is the velocity field, and u, w, and $\boldsymbol{e}_r$, $\boldsymbol{e}_z$ are the radial and axial velocity components and the corresponding unit vectors, respectively. In equation (2.2), $\boldsymbol{T} = -p\boldsymbol{I} + [\boldsymbol{\nabla}\boldsymbol{u} + (\boldsymbol{\nabla}\boldsymbol{u})^{\mathrm{T}}]$ is the stress tensor for an incompressible Newtonian liquid, $\boldsymbol{I}$ is the standard identity tensor, $p(\boldsymbol{x}, t)$ is the pressure field. Since we make use of the arbitrary Lagrangian-Eulerian (ALE) method, the deformable domain $\boldsymbol{x}(\boldsymbol{X}, t) \in \mathcal{V}(t)$ is parametrised by the initial position $\boldsymbol{X} = \boldsymbol{x}(\boldsymbol{X}, 0) \in \mathcal{V}(0)$, and the local time derivatives are evaluated in the spatial reference frame as

$$\frac{\partial \boldsymbol{u}}{\partial t} = \frac{\partial \hat{\boldsymbol{u}}}{\partial t} - \frac{\partial \boldsymbol{x}}{\partial t}\cdot\boldsymbol{\nabla}\boldsymbol{u} \qquad \text{at } \mathcal{V}, \tag{2.3}$$

where $\hat{\boldsymbol{u}}(\boldsymbol{X}, t) = \boldsymbol{u}(\boldsymbol{x}, t)$ is the velocity in the material reference frame.

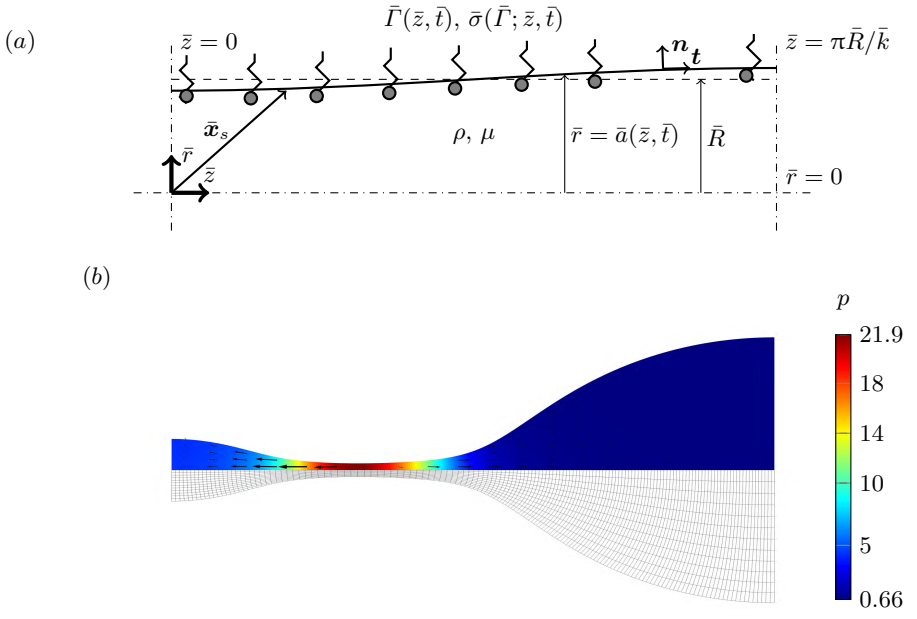

Figure 1: (Colour online) (*a*) Dimensional sketch of the flow configuration. (*b*) Example of a liquid thread approaching pinch-off for $La = 0.01$, $\beta = 1$, $\epsilon = 10^{-3}$ and $k = k_m = 0.516$ at time $t = 123$. The contour map represents the dimensionless pressure field p, and the arrows show the dimensionless velocity field $\boldsymbol{u}$, both at the top, while the deformed mesh is shown at the bottom.

Since the interface $\partial\mathcal{V}$ is coated with surfactant, a surface transport equation is needed for $\Gamma(\boldsymbol{x},t)$,

$$\frac{\partial\Gamma}{\partial t} + \boldsymbol{\nabla}_s\cdot(\Gamma\,\boldsymbol{u}_s) = 0 \qquad \text{at } \partial\mathcal{V}, \tag{2.4}$$

where $\boldsymbol{u}_s = \boldsymbol{u}(\boldsymbol{x}_s)$ is the liquid velocity at the interface, and $\boldsymbol{x}_s$ represents any position at the surface $\boldsymbol{x}_s(\boldsymbol{X}_s,t) \in \partial\mathcal{V}(t)$, which is parametrised by its initial position $\boldsymbol{X}_s = \boldsymbol{x}_s(\boldsymbol{X}_s,0) \in \partial\mathcal{V}(0)$. Here $\boldsymbol{\nabla}_s = \boldsymbol{I}_s\cdot\boldsymbol{\nabla}$ is the surface gradient operator, where $\boldsymbol{I}_s = \boldsymbol{I} - \boldsymbol{nn}$ is the surface projection tensor and $\boldsymbol{n}$ is the outer unit normal vector at the surface. The local time derivatives at the interface are evaluated in the spatial reference frame as

$$\frac{\partial\Gamma}{\partial t} = \frac{\partial\hat{\Gamma}}{\partial t} - \frac{\partial\boldsymbol{x}_s}{\partial t}\cdot\boldsymbol{\nabla}_s\Gamma \qquad \text{at } \partial\mathcal{V}, \tag{2.5}$$

where $\hat{\Gamma}(\boldsymbol{X}_s,t) = \Gamma(\boldsymbol{x}_s,t)$ is the concentration of surfactant in the material frame of reference, which is needed in order to be implemented with the ALE method that is used in the present work. The reader is referred to the works of Stone (1990), Wong *et al.* (1996) and Pereira & Kalliadasis (2008) for further details on the time derivative of a surface quantity†.

Note that the surface diffusion of surfactant has been neglected in the transport equation (2.4). Indeed, in the present work we only consider the limit where the surface Péclet number $Pe_s = U_{sc}\bar{R}/D_s \to \infty$, where D_s is the surface diffusion coefficient and U_{sc}

† Note that $\boldsymbol{u}_s$ does not have the same definition here than in Stone (1990), Wong *et al.* (1996) and Pereira & Kalliadasis (2008), where it corresponds to the tangential component of the fluid velocity at the interface, $\boldsymbol{I}_s\cdot\boldsymbol{u}$

is the characteristic liquid velocity at the free surface. The correct scaling for U_{sc} depends on the value of La. In the limit of dominant inertia, $La \gg 1$, the appropriate velocity scale is the capillary velocity, $[\sigma_0/(\rho\bar{R}^3)]^{1/2}$, so that $Pe_s = [\sigma_0\bar{R}/(\rho D_s^2)]^{1/2}$. For instance, if we consider a water thread of radius within the range 1-100 μm, the corresponding Laplace numbers lie in the range $10^2 \lesssim La \lesssim 10^4$. Typical values of D_s for SDS, SB12 and other monomers in aqueous solution are within the range $10^{-9} \lesssim D_s \lesssim 10^{-8}$ m^2 s^{-1} when Γ is below the critical micelle concentration (CMC) (Siderius *et al.* 2002), providing values of the surface Péclet number in the range $10^4 \lesssim Pe_s \lesssim 10^5$. Therefore, in configurations where $La \gg 1$, it is expected that surface diffusion has a very small effect. In the opposite limit of dominant viscous forces, $La \lesssim 1$, the appropriate velocity scale is the visco-capillary velocity, σ_0/μ, leading to $Pe_s = \sigma_0\bar{R}/(\mu D_s)$. Considering, for instance, a polydimethylsiloxane silicon oil of dynamic viscosity in the range 0.1-10 Pa s, density $\rho \approx 970$ kg m^{-3} and surface tension $\sigma_0 \approx 21.1$ mN m^{-1}, the Laplace number takes values in the range $10^{-4} \lesssim La \lesssim 1$. Although we are not aware of experimental studies reporting the typical values of D_s in highly viscous solutions, if we assume that they are of the same order as those in aqueous solutions, the Péclet number lies in the range $1 \lesssim Pe_s \lesssim 10^6$. It is thereby deduced that, when $La \lesssim 1$, there may be cases where surface diffusion cannot be neglected in the analysis. Therefore, although the influence of surface diffusion on the satellite droplet formation process is not addressed in the present work, it clearly deserves further study, particularly in the case of highly viscous threads.

The presence of surfactant at the interface modifies σ by decreasing its value as Γ increases, and thus the stress balance at the interface takes the following form in the limit $\mathscr{B}_\mu \ll 1$, $\mathscr{B}_\kappa \ll 1$ (Martínez-Calvo & Sevilla 2018),

$$\boldsymbol{T}\cdot\boldsymbol{n} = \boldsymbol{\nabla}_s\sigma - \boldsymbol{n}(\boldsymbol{\nabla}_s\cdot\boldsymbol{n})\sigma \qquad \text{at } \partial\mathcal{V}\,, \tag{2.6}$$

where the viscous stress exerted by the ambient fluid on the interface has been neglected and the ambient pressure p_a has been set to zero without loss of generality. Additionally, the kinematic condition must also hold at the interface

$$\boldsymbol{u}_s\cdot\boldsymbol{n} = \frac{\partial\boldsymbol{x}_s}{\partial t}\cdot\boldsymbol{n} \qquad \text{at } \partial\mathcal{V}. \tag{2.7}$$

Finally, an equation of state that relates the surface tension, σ, with the surface concentration of surfactant, Γ, is also needed. Surface-active molecules at the interface induce a surface pressure $\bar{\Pi}$ which depends on the surfactant concentration, $\bar{\Pi} = \bar{\Pi}(\bar{\Gamma})$. The surface pressure is defined as the difference in the surface tension due to the presence of surfactant, $\bar{\Pi}(\bar{\Gamma}) = \sigma_{\text{clean}} - \bar{\sigma}(\bar{\Gamma})$, and thus $\boldsymbol{\nabla}_s\bar{\Pi} = -\boldsymbol{\nabla}_s\bar{\sigma}$. In addition, the Gibbs elasticity E relates the changes of interface area, $\bar{A}$, with the surface pressure through the surface compressibility $1/E = -(1/\bar{A})(\partial\bar{A}/\partial\bar{\Pi})_{\bar{T}}$, where $\bar{T}$ is the temperature at the interface, which is assumed to remain constant. Hence,

$$E = -\bar{A}\frac{\partial\bar{\Pi}}{\partial\bar{A}} = \bar{A}\frac{\partial\bar{\sigma}}{\partial\bar{A}} = -\bar{\Gamma}\frac{\partial\bar{\sigma}}{\partial\bar{\Gamma}}, \tag{2.8}$$

where in the last equation it has been taken into account that, in the insoluble case considered in the present work, the number of surfactant molecules is conserved at the interface. Equation (2.8) can be used to relate $\bar{\sigma}$ and $\bar{\Gamma}$,

$$\boldsymbol{\nabla}_s\bar{\sigma} = \frac{\partial\bar{\sigma}}{\partial\bar{\Gamma}}\boldsymbol{\nabla}_s\bar{\Gamma} = -\frac{E}{\bar{\Gamma}}\boldsymbol{\nabla}_s\bar{\Gamma}. \tag{2.9}$$

Making $\bar{\sigma}$ and $\bar{\Gamma}$ dimensionless with σ_0 and Γ_0, respectively, equation (2.9) finally yields

the dimensionless equation of state

$$\sigma = 1 - \beta \ln \Gamma, \tag{2.10}$$

where $\beta = E/\sigma_0$ is the so-called elasticity parameter, also referred to as the Marangoni number (Champougny *et al.* 2015). Note that, in the limit of small surface concentration variations around the initial value, $\bar{\Gamma} = \Gamma_0 + \delta\bar{\Gamma}$, with $\delta\bar{\Gamma} \ll \Gamma_0$, one has $\Gamma = 1 + \delta\Gamma$ with $\delta\Gamma \ll 1$, and the equation of state (2.10) can be linearised to yield $\sigma = 1 - \beta\delta\Gamma$, which is equivalent to the equation of state employed by Dravid *et al.* (2006). However, it is important to emphasise that the relative variations of Γ during the thread break-up process are not small, as demonstrated in §3. Therefore, the use of a linearised equation of state introduces considerable errors and is not justified. The surface stress balance (2.6) can be rewritten in terms of Γ as

$$\boldsymbol{T}\cdot\boldsymbol{n} = -\beta\,\boldsymbol{\nabla}_s(\ln\Gamma) - \boldsymbol{n}\,(\boldsymbol{\nabla}_s\cdot\boldsymbol{n})\,(1-\beta\ln\Gamma) \qquad \text{at } \partial\mathcal{V}, \tag{2.11}$$

which, together with equations (2.1)–(2.5) and (2.7), form a closed system to determine $\boldsymbol{u}$, p, Γ and $\boldsymbol{x}_s$.

Concerning the computational domain and the corresponding boundary conditions, in the temporal approach adopted herein we only consider half a perturbation wavelength subjected to the following symmetry conditions at $z = \{0, \pi/k\}$, where k is the dimensionless axial wavenumber,

$$w = 0, \quad \frac{\partial u}{\partial z} = 0, \quad \frac{\partial \Gamma}{\partial z} = 0, \tag{2.12}$$

together with the axisymmetry condition at $r = 0$,

$$\frac{\partial w}{\partial r} = 0, \quad u = 0. \tag{2.13}$$

Finally, regarding the initial conditions imposed at $t = 0$, we perturb the position of the liquid cylinder with a harmonic disturbance of amplitude ϵ,

$$\boldsymbol{x}_s = z\boldsymbol{e}_z + [R - \epsilon\cos(kz)]\boldsymbol{e}_r, \tag{2.14}$$

where $R = (1 - \epsilon^2/2)^{1/2}$ is a dimensionless radius defined in terms of ϵ, such that the liquid volume remains constant as ϵ varies (Ashgriz & Mashayek 1995). We also assume that the liquid thread is initially at rest† and that the surfactant concentration is uniform,

$$\boldsymbol{u}(\boldsymbol{x}, 0) = \boldsymbol{0}, \quad \Gamma(\boldsymbol{x}_s, 0) = 1. \tag{2.15}$$

Note that the assumption of a uniform initial concentration of surfactant is a good approximation, since our main results have been obtained in the limit $\epsilon \ll 1$ in which the deviations from a uniform concentration can be neglected.

The problem depends on four dimensionless parameters, namely the Laplace number, La, the elasticity parameter, β, the axial wavenumber, k, and the amplitude of the initial perturbation, ϵ. However, in the present work we are concerned with the unforced break-up of cylindrical threads due to small radius disturbances. Therefore, all the results were obtained by setting $k = k_m$, where $k_m(La, \beta)$ is the most unstable wavenumber

† Note that, as explained in §1, our results also apply to liquid jets moving with uniform velocity profile U with respect to the injector reference frame, provided that $U \gg U_\sigma$, where U_σ is the speed of small-amplitude capillary waves. If the latter condition is satisfied, the spatial evolution of the jet is obtained by the downstream advection of the temporal results presented herein with a uniform velocity U. In particular, the jet break-up length is given by Ut_b in a first approximation.

(see §3.1). Moreover, it will be shown that, in the small-disturbance limit, $\epsilon \ll 1$, the only result that depends on ϵ is the break-up time of the thread, $t_b(La, \beta, \epsilon)$. However, our results have revealed that the functional dependence of t_b can be split into a contribution predicted by linear theory in explicit form, $t_{b,L}(La, \beta, \epsilon)$, plus a nonlinear correction, $\Delta t_{\mathrm{NL}}(La, \beta)$, which does not depend on ϵ. Consequently, only two independent dimensionless parameters appear in our formulation, namely La and β.

To perform the numerical simulations, the liquid domain $0 \leqslant r \leqslant a(z,t), 0 \leqslant z \leqslant \pi/k$ is partitioned into a rectangular finite-element mesh which is dynamically deformed using the ALE method. In particular, the displacement field, $\boldsymbol{x} - \boldsymbol{X}$, is enforced to satisfy the Laplace equation, and the normal mesh velocity, $\dot{\boldsymbol{x}}_s = \boldsymbol{n}\boldsymbol{n} \cdot \boldsymbol{v}$, solves the kinematic condition (2.7). To that end, equations (2.1)–(2.4), together with the boundary and initial conditions (2.12)–(2.15), are written in weak form following the methodology described by Rivero-Rodríguez & Scheid (2018*a*,*b*), and the spatial discretisation is carried out using the finite element method (FEM) provided by COMSOL, where Lagrange linear (P1) elements are used for p, and quadratic (P2) elements for $\boldsymbol{x}$, $\boldsymbol{u}$ and Γ. The time discretisation was performed using the first-order backward Euler method with adaptative time stepping. Figure 1(*b*) shows a representative deformed mesh for a simulation with $La = 0.01$, $\beta = 1$, $\epsilon = 10^{-3}$ and $k = k_m = 0.516$ at the time $t = 123$, together with the pressure field as a contour plot and the velocity field represented by arrows. All the results reported were carefully checked to be mesh-independent, with an integration tolerance of the order of 10^{-6}–10^{-7}. In addition, it was checked that the relative variations of liquid volume and surfactant mass where smaller than 10^{-5} during each simulation.

3. Results and discussion

Since we are interested in the spontaneous break-up of the surfactant-laden thread, all the results were computed from an initial condition where the liquid cylinder is perturbed with the wavenumber of maximum amplification, $k_m(La, \beta)$. Hence, the results of a linear stability analysis are first summarised in §3.1 to obtain k_m and ω_m, the latter being the maximum temporal growth rate. Note that k_m is needed to define the initial geometry and the initial condition (2.14), while ω_m is used to compute the nonlinear correction to the linear break-up time, which is defined in §3.2. In addition, the linear theory has also been used to validate the numerical code by comparing the associated maximum temporal growth rate, ω_m, with the results extracted from the numerical simulations during the initial transient of exponential amplitude growth. Sections §3.2 and 3.3 are devoted to analyse the nonlinear break-up and the satellite formation dynamics, separating the weak-elasticity limit, and the surfactant-laden case. To that end, we have performed direct numerical simulations of equations (2.1)–(2.15) until times very close to pinch-off. In particular, we report a parametric study for different values of La and β, computing the volume of the satellite droplet, the mass of surfactant trapped at its interface, the satellite shape at pinch-off, and the break-up time.

At this point, it has to be pointed out that a similar phenomenology had been previously reported by Dravid *et al.* (2006) for $La = 0.01$ and 100, although using the unrealistic linear equation of state $\sigma(\Gamma) = 1 - \beta(\Gamma - 1)$. In addition, these authors did not consider the natural break-up of the thread, since the disturbance wavenumber k was restricted to fixed values different from the most amplified one, k_m. Besides, neither V_{sat} nor Σ_{sat} were computed, and no detailed physical analysis accompanied the results.

3.1. *Linear stability analysis*

To obtain the dispersion relation $D(\omega, k) = 0$ relating the temporal growth rate ω and the axial wavenumber k, all the flow variables are slightly perturbed around a uniform stationary state and decomposed as temporal normal modes,

$$(u, w, p, a, \sigma, \Gamma) = (0, 0, 1, 1, 1, 1) + \epsilon(\hat{u}, \hat{v}, \hat{p}, \hat{a}, \hat{\sigma}, \hat{\Gamma}) \exp(ikz + \omega t). \tag{3.1}$$

Introducing (3.1) into the system (2.1)–(2.4) and keeping terms proportional to ϵ, the following dispersion relation is obtained:

$$\begin{aligned} &La\,\omega^2 F(k) - k^2(1-k^2) + \beta k^2[1 + F(k)(F(\tilde{k}) - 2)] \\ &+ \frac{k^4}{La}\left[4 - \frac{\beta}{\omega}\left(2 - \frac{1-k^2}{\omega}\right)\right][F(k) - F(\tilde{k})] + 2\omega k^2(2F(k) - 1) = 0, \end{aligned} \tag{3.2}$$

where $\tilde{k}^2 = k^2 + La\,\omega$ and $F(x) = xI_0(x)/I_1(x)$. Here, $I_n(x)$ denotes the nth-order modified Bessel function of the first kind. Note that the dispersion relation (3.2) is exactly the same as the one deduced by Timmermans & Lister (2002), and is also a particular case of the one provided by Martínez-Calvo & Sevilla (2018) in the limit of negligible surface viscosities. The Rayleigh–Chandrasekhar dispersion relation is recovered when $\beta \to 0$ (Rayleigh 1892; Chandrasekhar 1961).

As shown experimentally by Goedde & Yuen (1970), and numerically by Mansour & Lundgren (1990) and Ashgriz & Mashayek (1995), a convenient way to compute the temporal growth rate of small disturbances is through the radius amplitude, extracted from the present simulations as $A(t) = (\max_z[a(z,t)] - \min_z[a(z,t)])/2$. Figure 2($a$) shows the temporal evolution of $A(t)$ in semi-logarithmic scale, extracted from two numerical simulations for an initial perturbation amplitude $\epsilon = 10^{-4}$, an elasticity parameter $\beta = 1$, and two values of the Laplace number, $La = 0.01$ and $La = 100$, close to the Stokes and Euler regimes, respectively. In each case, the most amplified wavenumber, $k_m(La, \beta)$, is used to build the initial condition. As expected due to the smallness of ϵ, figure 2(a) shows that during most of the time the amplitude grows exponentially, i.e. $A \propto \exp(\omega_m t)$, and thus the maximum temporal growth rate, $\omega_m(La, \beta)$, can be easily computed as the slope of the linear region in the semi-logarithmic plot, $\omega_m = \mathrm{d}\ln(A)/\mathrm{d}t$. It can also be deduced from figure 2(a) that there is an initial transient during which the growth of $A(t)$ is not exponential, what can be explained by the fact that the initial conditions in the numerical simulations are imposed on the shape of the interface, but disregard the associated disturbances in the velocity, pressure and surfactant concentration fields. As shown in figure 2(b), this procedure was used to obtain ω for different values of k (symbols), and the results are compared with the amplification curves $\omega(k)$ computed from the dispersion relation (3.2) (solid lines), obtaining an excellent agreement that validates the numerical code in the linear regime. Finally, figures 2(c, d) show the isocontours of k_m and ω_m, respectively, as a function of La and β extracted from equation (3.2), whose values will be used hereafter.

3.2. *Satellite formation regimes and transitions in the* (La, β) *parameter plane*

Let us first present the structure of the (La, β) parameter plane in terms of the satellite formation process. To that end, we conducted an exhaustive parametric study in which the Laplace and elasticity parameters were varied in small steps within wide ranges, namely $0.01 \leqslant La \leqslant 100$ and $0 \leqslant \beta \leqslant 1$. Thus, for each pair of values of La and β, we simulated the instability-driven time evolution of the thread from an initial condition with $\epsilon \ll 1$ until a time t_b very close to break-up. In total, around 10^4 time-dependent

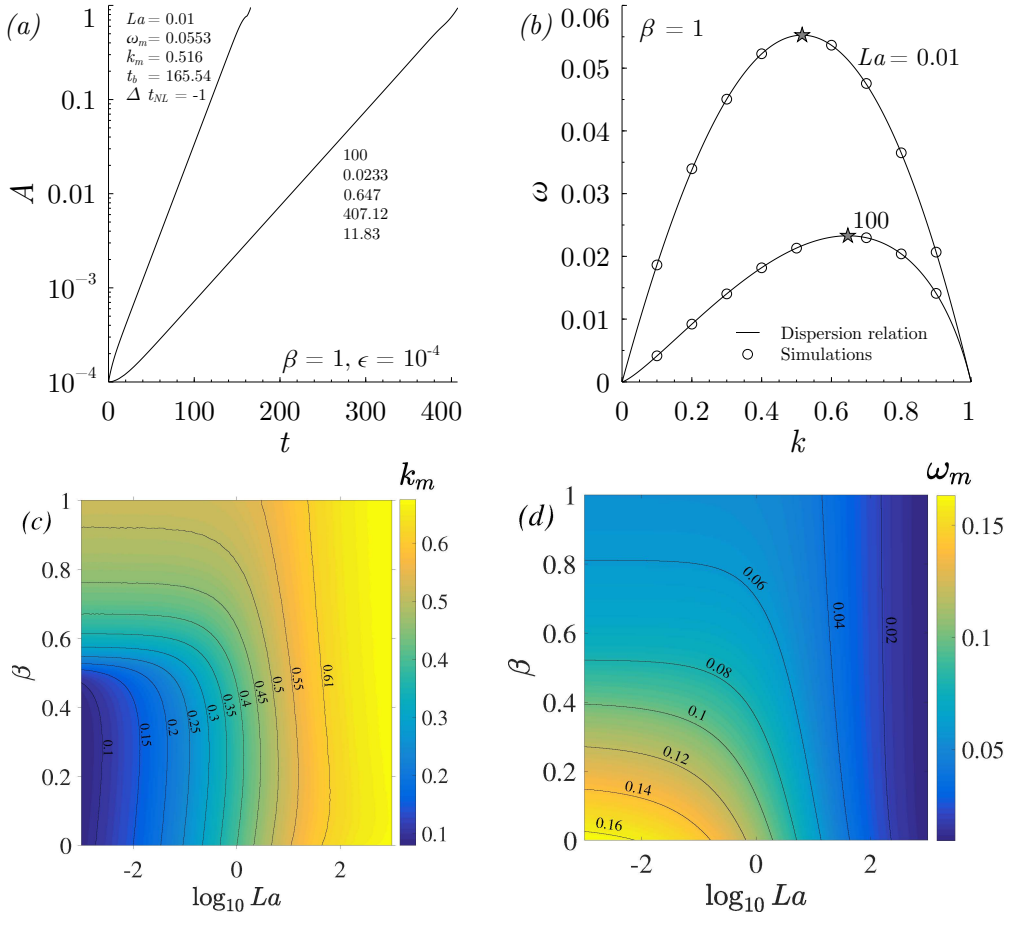

Figure 2: (Colour online) (a) Semi-logarithmic plot of the radius amplitude $A(t)$ as a function of time, extracted from two numerical simulations for $\epsilon = 10^{-4}$, $\beta = 1$ and two values of the Laplace number, namely $La = (0.01, 100)$. The corresponding optimal wavenumbers, $k_m(La, \beta)$, highlighted in (b) with stars, are used to build the initial conditions, and their values are indicated near each curve together with the associated linear temporal growth rates, $\omega_m(La, \beta)$ and La. (b) Temporal growth rate ω as a function of the axial wavenumber k, computed with the dispersion relation (3.2) (solid lines) and with the numerical simulations (circles), for $\beta = 1$ and two different values of $La = (0.01, 100)$, indicated near each curve. The maximum growth rates ω_m computed in (a) are marked with stars. (c) Isocontours of the most amplified wavenumber $k_m(La, \beta)$ and its corresponding growth rate $\omega_m(La, \beta)$ in (d).

simulations were carried out to characterise the (La, β) parameter plane shown in figures 3 and 5.

At this point, it is important to emphasise that the fate of the main and satellite drops after pinch-off is outside the scope of the present work, and therefore we do not explore the possible successive break-up events that may take place and lead to the formation of sub-satellites. Keeping this in mind, we have extracted the satellite volume at the last numerical step, $t = t_b$. Normalising its value with the total volume provides the definition

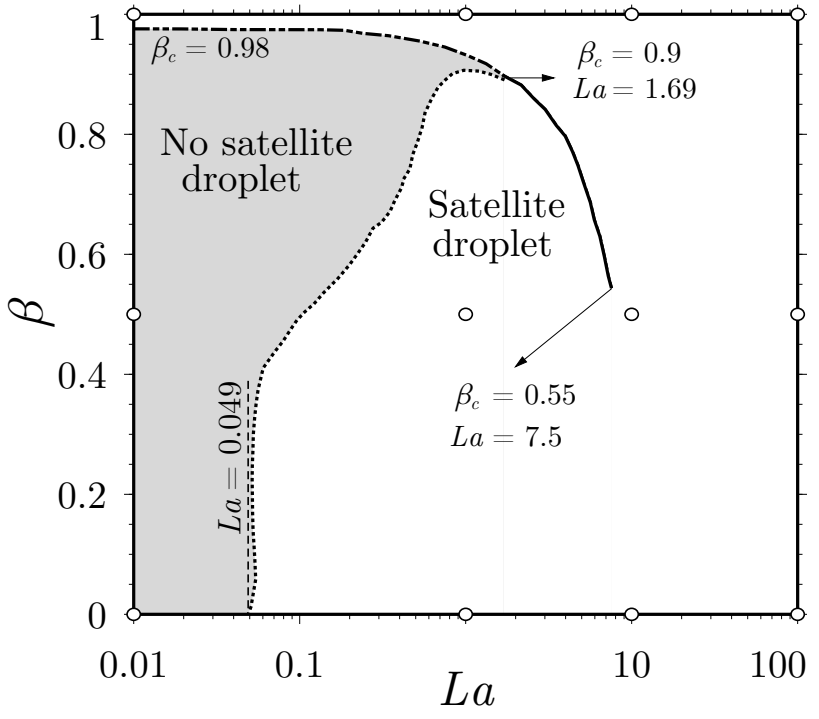

Figure 3: The different regions and transition curves identified in the (La, β) parameter plane. A satellite droplet is present at pinch-off in the unshaded area, while no satellite is formed in the shaded region. The dotted line represents the transition between the break-up of a thin filament (shaded region) and the break-up away from the symmetry plane, $z = 0$, leaving a satellite droplet in between (unshaded region), and was computed for convenience as the isocontour of constant dimensionless satellite volume $V_{\rm sat} = 3 \times 10^{-5}$. Abrupt transitions take place along the dash-dotted and solid lines, $\beta = \beta_c(La)$, in which the satellite volume experiences a discontinuity at β_c. In the case of the dash-dotted line, defined for $La < 1.69$, the volume of the satellite suddenly increases from zero in the shaded region, $\beta < \beta_c$, to a finite value in the unshaded region, $\beta > \beta_c$. In the case of the solid line, defined in the range $1.69 < La < 7.5$, the volume suddenly increases from a nonzero value for $\beta < \beta_c$, to a larger value for $\beta > \beta_c$. For $La > 7.5$, the satellite volume is a continuous function of β. The circles correspond to the values of La and β of the shapes just before pinch-off shown in figure 4.

$$V_{\rm sat} = \frac{\int_0^{z_{\rm min}} a^2 {\rm d}z}{\int_0^{\pi/k_m} a^2 {\rm d}z}, \tag{3.3}$$

where $z_{\rm min}$ is the axial position where the liquid column reaches its minimum radius, $a_{\rm min}$, at $t = t_b$. A more common measure of the satellite size is its equivalent radius, $R_{\rm sat}$, which is the radius of a spherical drop of the same volume as the satellite (Rutland & Jameson 1971; Mansour & Lundgren 1990; Ashgriz & Mashayek 1995; Mashayek & Ashgriz 1995). All the results reported herein in terms of $V_{\rm sat}$ can be easily converted to $R_{\rm sat}$ through the equation $R_{\rm sat} = [3\pi V_{\rm sat}/(2k_m)]^{1/3}$. Following the same procedure, we have also computed the mass of surfactant trapped at the satellite surface which,

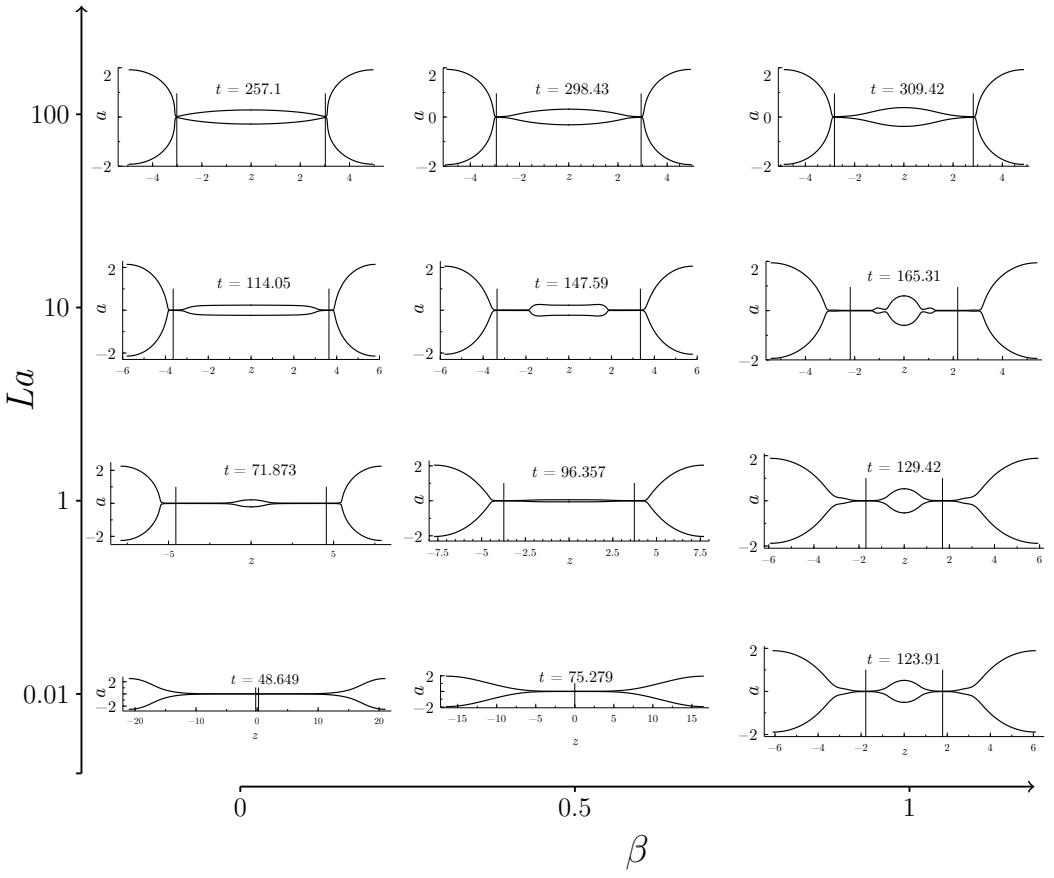

Figure 4: The satellite shapes just prior to pinch-off in the (La, β) parameter plane (see open circles in figure 3). The vertical lines indicate the axial positions, $z_{\min}$, of the minimum thread radii, $a_{\min}$.

normalised with the total mass of surfactant, provides the definition

$$\Sigma_{\rm sat} = \frac{\int_0^{z_{\min}} a\Gamma\sqrt{1+\left(\frac{\partial a}{\partial z}\right)^2}\mathrm{d}z}{\int_0^{\pi/k_m} a\Gamma\sqrt{1+\left(\frac{\partial a}{\partial z}\right)^2}\mathrm{d}z}. \tag{3.4}$$

We would like to point out that, since $V_{\rm sat}$ and $\Sigma_{\rm sat}$ are obtained when $a_{\min} \lesssim 8\times10^{-3}$, the sensitivity of these magnitudes to the exact value of $a_{\min}$ is negligible, such that both represent very robust measures. Similarly, the corresponding breakup time t_b is barely sensitive to the value of $a_{\min}$.

In contrast with $V_{\rm sat}$ and $\Sigma_{\rm sat}$, which do not depend on the initial amplitude in the limit $\epsilon \ll 1$, the break-up time is a function of the form $t_b(La, \beta, \epsilon)$ such that $t_b \to \infty$ as $\epsilon \to 0$. Indeed, the break-up time can be easily estimated from linear theory through the equation $a_{min}(t) \sim 1 - \epsilon\exp(\omega_m t)$, where ω_m is the growth rate associated with the most amplified wavenumber k_m shown in figures 2 (c, d), leading to the estimation $t_b \sim \ln(\epsilon^{-1})/\omega_m$. Based on the latter result, we define the nonlinear correction to the

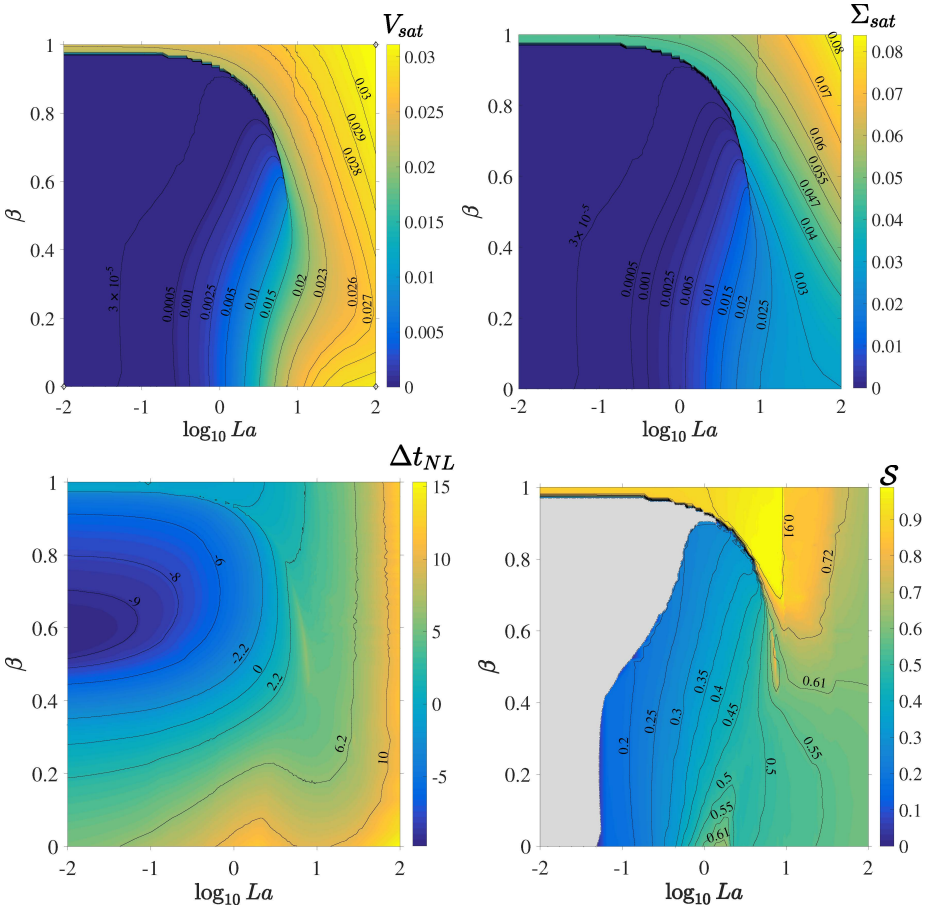

Figure 5: Isocontours in the (La, β) parameter plane of (a) the normalised satellite volume $V_{\rm sat}$, (b) the normalised mass of surfactant trapped at its interface $\Sigma_{\rm sat}$, (c) the nonlinear correction to the break-up time, $\Delta t_{\rm NL}$, and (d) the sphericity of the satellite droplet, $\mathcal{S}$.

linear break-up time as

$$\Delta t_{\rm NL} = t_b - \frac{\ln(\epsilon^{-1})}{\omega_m}, \tag{3.5}$$

where t_b is obtained by extrapolating a_{min} to zero using the last few computed time steps. Unlike t_b, $\Delta t_{\rm NL}$ only depends on La and β, but not on ϵ, provided only that $\epsilon \ll 1$. The latter fact is demonstrated in §3.3. Finally, we have also computed the sphericity of the satellite droplet at pinch-off as

$$\mathcal{S} = \frac{2\left(\frac{3}{4}\int_0^{z_{\rm min}} a^2 {\rm d}z\right)^{2/3}}{\int_0^{z_{\rm min}} a\sqrt{1+\left(\frac{\partial a}{\partial z}\right)^2}{\rm d}z}, \tag{3.6}$$

which is the ratio between the surface of a sphere of the same volume as the satellite and its actual surface. The quantification of the satellite formation process will be based on the four functions $V_{\rm sat}$, $\Sigma_{\rm sat}$, $\Delta t_{\rm NL}$ and $\mathcal{S}$, extracted from the numerical simulations. These four functions only depend on La and β when ϵ is sufficiently small, as will be

demonstrated in §3.3. Thus, the main results reported herein have been computed in the limit $\epsilon \to 0$.

The structure of the (La,β) parameter plane is summarised in figures 3 and 4 in terms of the satellite formation process. In particular, figure 3 shows the different regions and transitions that take place, and figure 4 displays several satellite shapes at the last computed numerical step just prior to pinch-off, whose associated values of La and β are indicated with circles in figure 3. In the latter figure, the unshaded region corresponds to situations in which, just prior to pinch-off, the two main drops are connected either by a satellite droplet (see e.g. the interface shape for $La = 100$ and $\beta = 0$ in figure 4), or by a liquid thread with a satellite droplet at its center (see e.g. the case for $La = 1$ and $\beta = 0$ in figure 4). On the contrary, the shaded region corresponds to cases where, at pinch-off, the two main drops are connected by a very thin thread of tiny volume whose detailed break-up behavior has been characterised in previous studies (see e.g. Kowalewski 1996). To delineate the *smooth transition* between thin threads and satellites for small and high enough values of La, respectively, the dotted line in figure 3 represents the isocontour $V_{\rm sat} = 3{\times}10^{-5}$, as a cut-off below which the satellite formed at the centre of the thread has a negligible volume compared to the thread (see e.g. the interface shape for $La = 0.01$ and $\beta = 0$ in figure 4). In contrast, the dash-dotted and solid lines represent a *discontinuous transition* at $\beta = \beta_c(La)$, that takes place within the range $0 < La < 7.5$, and above which $V_{\rm sat}$ and $\Sigma_{\rm sat}$ increase abruptly. In particular, for $La < 1.69$, the dashed-dotted line corresponds to a sharp transition from a negligible satellite droplet (shaded region), i.e. $V_{\rm sat} < 3 \times 10^{-5}$, when $\beta < \beta_c$, to a non-zero satellite droplet (unshaded region) when $\beta > \beta_c$. The latter behaviour is clearly illustrated by comparing in figure 4 the interface shape for $La = 0.01$ and $\beta = 0.5 < \beta_c$, with that for $La = 0.01$ and $\beta = 1 > \beta_c$. Similarly, the solid line defines a discontinuous transition when $1.69 < La < 7.5$, where $V_{\rm sat}$ and $\Sigma_{\rm sat}$ increase abruptly but from a certain non-zero value when $\beta < \beta_c$ to a higher value when $\beta > \beta_c$. For $La \ll 1$, the critical elasticity reaches a plateau, namely $\beta_c = 0.98$, and decreases monotonically when La increases, reaching a value of $\beta_c = 0.55$ at $La = 7.5$. For larger values of La the discontinuous transition disappears. Both the continuous and the discontinuous transitions coexist in the range $0.049 < La < 1.69$.

From figures 3 and 4 it is deduced that, although the physical mechanisms are different, both the liquid inertia and the interfacial elastic stress favour the formation of satellites. In particular, surface elasticity tends to form spherical-shaped satellites at pinch-off, whereas the increase of the liquid inertia generates oval-shaped satellites. In the set of shapes close to pinch-off shown in figure 4, the discontinuous transition is observed for $La = 0.01$ and 1, as β increases. For $La = 10$, a continuous transition of the thread shape is observed as β increases. Finally, for $La = 100$, the upper row evidences that the influence of the elastic stress on the shape of the thread is much weaker when La is high enough. The physics underlying these transitions can be explained in terms of the competition and the coupling between the liquid inertia, the viscous stress, the surface tension, and the interfacial elastic stress. The competition between these forces will be discussed in §3.3, based on the trends exhibited by the functions $V_{\rm sat}$, $\Sigma_{\rm sat}$, $\Delta t_{\rm NL}$ and $\mathcal{S}$, and also by analysing the temporal evolution of the interface shapes starting from small disturbances, depending on the values of La and β.

3.3. *Nonlinear dynamics of a surfactant-laden interface: satellite drop formation*

To unveil the effect of liquid inertia, viscous stresses and surface elasticity on the satellite droplet formation regimes, here we present and discuss the quantitative results of the detailed numerical analysis that has been carried out in the present work.

Figure 5 shows the isocontours of $V_{\rm sat}$, $\Sigma_{\rm sat}$, $\Delta t_{\rm NL}$ and $\mathcal{S}$ in the (La, β) parameter

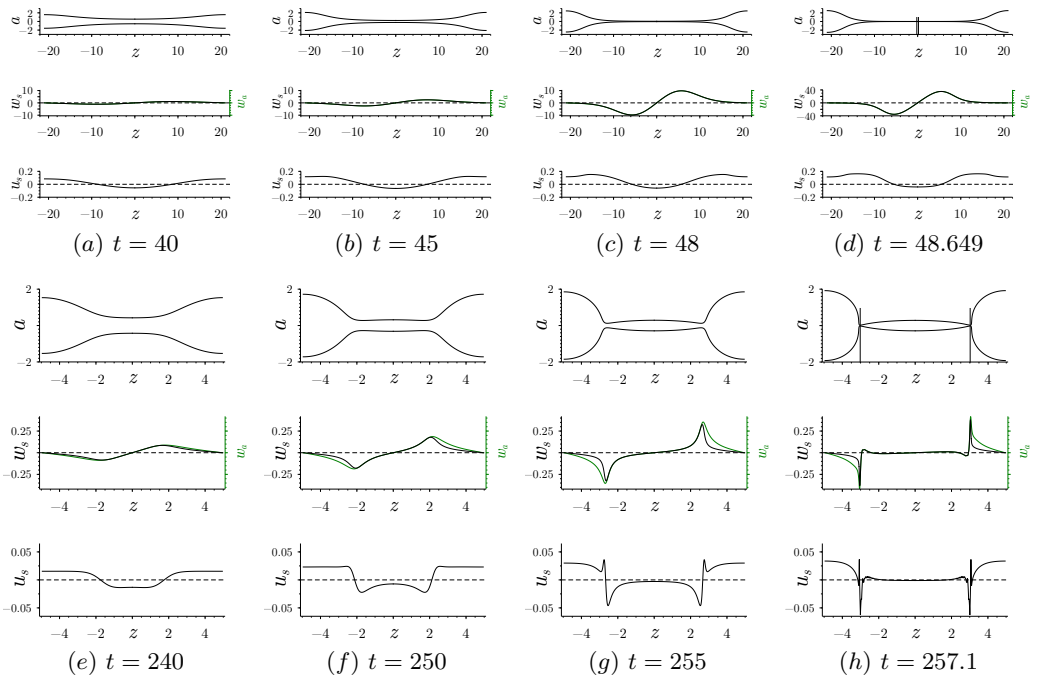

Figure 6: Temporal evolution of the liquid thread radius a (upper row), of the axial velocities at the free surface, w_s, and at the axis, w_a (middle row) and the radial surface velocity u_s (bottom row), for $\epsilon = 10^{-3}$, $\beta = 0$, (*a–d*) $La = 0.01$, $k = k_m = 0.150$, and (*e–h*) $La = 100$, $k = k_m = 0.635$. The vertical lines in each last snapshot indicate the axial position $z_{\min}$ of minimum radii $a_{\min}$.

plane. We first observe that, at the discontinuous transition that occurs for $La < 7.5$, the value of $V_{\rm sat}$ increases from 0–1.5 % to 2–2.3 %, whereas $\Sigma_{\rm sat}$ increases from 0–1.5 % to 3.5–4.7 %. In contrast, for $La > 7.5$ or $\beta > \beta_c(La)$, the values of $V_{\rm sat}$, $\Sigma_{\rm sat}$, $\Delta t_{\rm NL}$ and $\mathcal{S}$ vary continuously.

As a first general observation, it is deduced from figure 5 that the linear theory may either underestimate or overestimate the break-up time, in a way that does not neccessarily coincide with the transitions in the satellite formation process. Indeed, t_b is underestimated for $La \gg 1$ independently of the value of β. However, for $La \ll 1$, t_b is overestimated for $0.28 \lesssim \beta \lesssim 1$, while it is underestimated outside this range. Regarding the sphericity $\mathcal{S}$, figure 5 confirms the trend deduced from figure 4: the most spherical satellite shapes, with $\mathcal{S} \gtrsim 0.9$, take place for $\beta \gtrsim 0.7$ and $La \lesssim 10$. In contrast, the shapes become most elongated, with $\mathcal{S} \lesssim 0.2$, when $\beta < \beta_c$ and $La \lesssim 0.1$.

3.3.1. *Analysis of the temporal evolution of clean interfaces*

To present the dynamics of satellite droplet formation, we will take as reference cases the two canonical temporal evolutions of clean interfaces ($\beta = 0$) illustrated in figure 6, for $La = 0.01$ in (*a–d*), close to the Stokes limit, and for $La = 100$ in (*e–h*), an almost inviscid case close to the Euler limit. Specifically, we plot snapshots at different times, indicated in the labels, of the jet radius a (upper rows), the axial surface velocity w_s (middle rows, black lines), the axial velocity at the centerline w_a (middle rows, green lines), and the radial surface velocity u_s (bottom rows). In both cases the initial disturbance amplitude

is very small, $\epsilon = 10^{-3}$, and thus the initial evolution is triggered by the Plateau–Rayleigh instability mechanism, and can be described with linearised theory. This initial stage is not shown in figure 6 for conciseness, but it can be appreciated in figure 2(a). The initial disturbance, of most amplified wavelength k_m, creates an axial capillary pressure gradient that induces a flow from the valley to the crest of the wave. The latter mechanism finally leads to the break-up of the liquid thread and the formation of two main drops with either a liquid thread or a satellite droplet in between.

A key feature that determines the nonlinear evolution of the destabilised thread is the fact that the axial curvature makes the capillary pressure gradient to be locally larger in the regions that connect the central part of the thread with the growing crests, as evidenced by the surface and axis velocities in the snapshot (f). This enhanced pressure gradient drives liquid towards the crests faster in the nearby regions than in the central part, and explains the appearance of two local minima in the jet radius for large enough values of La, as can be clearly appreciated in snapshots (f,g) for $La = 100$. In addition, the axial position of the minimum radii $z_{\min}$ is advected with the flow along with the maximum pressure gradient, i.e. towards higher values of z as time advances. These two local minima become the two neck regions where pinch-off takes place, leading to the formation of an oval-shaped satellite droplet, as can be observed in snapshot (h). This scenario applies to cases where $La \gg 1$ (figure 6 e–h), for which the viscous stress is negligible, and the capillary pressure gradient is entirely transferred to liquid inertia leading to a self-accelerated process.

In contrast, when $La \ll 1$ (figure 6 a–d), the viscous dissipation inhibits the growth of higher harmonics, and larger pressure gradients are needed to overcome the viscous damping, as was already pointed out by Ashgriz & Mashayek (1995). Hence, the axial movement of the minimum radius is delayed by the viscous stress, since it weakens the capillary pressure and the concomitant liquid advection. Consequently, the central region shrinks almost uniformly until the last instants before break-up, giving rise to long and thin filaments without the formation of appreciable satellite droplets before detachment. Notice also that, for $La \ll 1$, the axial velocities at the centreline, w_a, and at the interface, w_s, are almost equal (green and black lines in figures 6 a–d, respectively), indicating that the radial profile of axial velocity inside the thread is nearly uniform at low Laplace numbers.

3.3.2. *Analysis of the temporal evolution of surfactant-laden interfaces*

To explain the different trends and transitions observed in figure 5, let us first focus on the effect of β for the particular cases of $La = 0.01$ and $La = 100$. Figure 7 shows $V_{\rm sat}$ (a,c), $\Sigma_{\rm sat}$ (b,d) and $\Delta t_{\rm NL}$ (insets in b and d), as functions of β for $La = 0.01$ in (a,b), and for $La = 100$ in (c,d). In addition, we have computed the results for several values of ϵ indicated in the legend of figure 7(a), with the aim at clearly establishing the limit of infinitesimal disturbances. In particular, figure 7 shows that $V_{\rm sat}$, $\Sigma_{\rm sat}$ and $\Delta t_{\rm NL}$ become independent of ϵ provided that $\epsilon \ll 1$, as stated before. Indeed, the insets in (a,c), which show the dependence of $V_{\rm sat}$ on ϵ, clearly demonstrate that the value of $V_{\rm sat}$ reaches the infinitesimal-disturbance plateau when $\epsilon \lesssim 0.1$. Figure 7 also displays the results obtained with the linear equation of state $\sigma = 1 - \beta(\Gamma - 1)$ (dotted line), instead of the nonlinear one (2.10). It is important to note that the use of the linear equation of state leads to substantial quantitative differences with respect to the nonlinear one (2.10). In particular, the linear equation underestimates the values of $V_{\rm sat}$ and $\Sigma_{\rm sat}$ considerably. We note also that we compared our numerical results using the linear equation of state with those reported by Dravid *et al.* (2006), finding very good agreement. However, their results were calculated for wavenumbers $k \neq k_m$, and the satellite droplet was measured

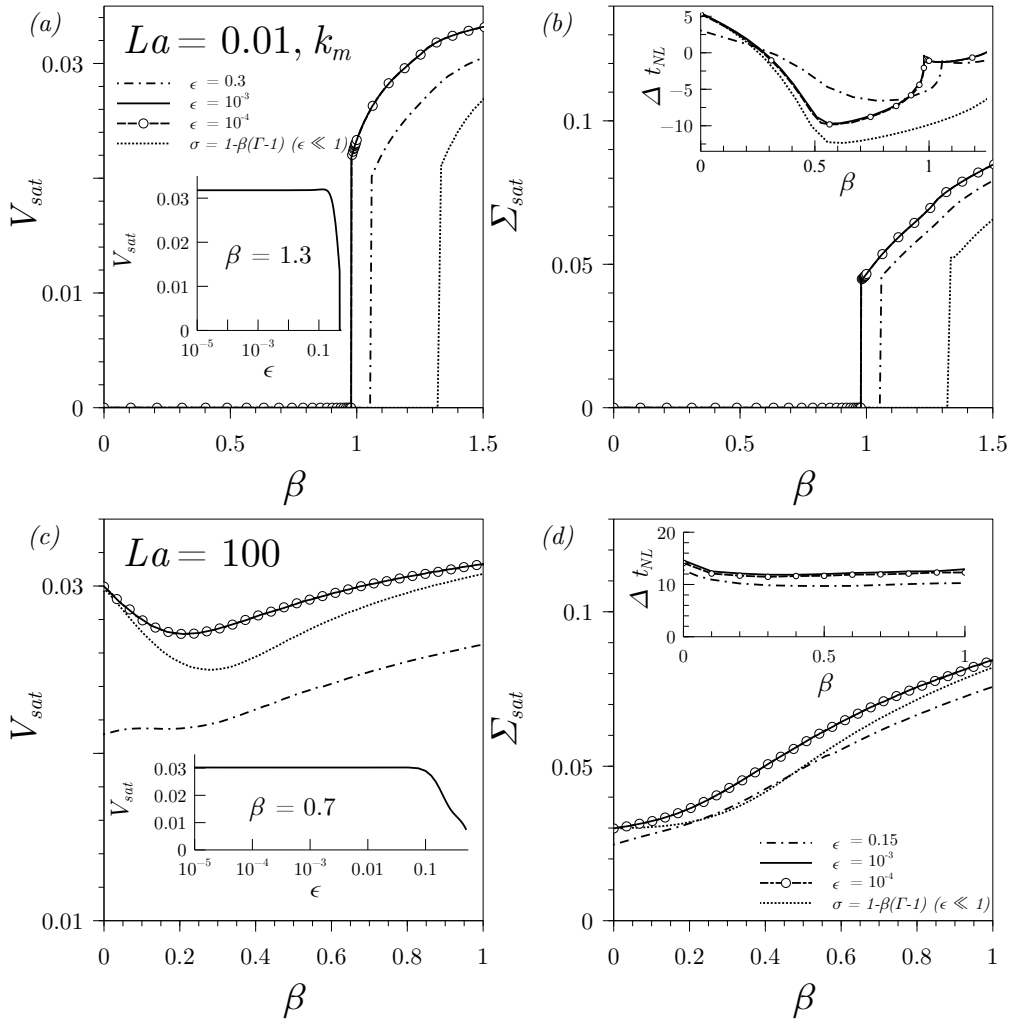

Figure 7: $V_{\rm sat}$ and $\Sigma_{\rm sat}$ as a function of β for (a,b) $La = 0.01$ and (c,d) $La = 100$, and for different values of the initial perturbation amplitude ϵ indicated in the legend. The dotted line represents the results of using the linear equation of state $\sigma = 1 - \beta(\Gamma - 1)$, finding analogous results as those drawn by Dravid *et al.* (2006). The insets show $V_{\rm sat}$ as a function of ϵ in logarithmic scale for (a) $\beta = 1.3$ and (c) $\beta = 0.7$, demonstrating that the final stage of the liquid thread just before pinch-off becomes independent of ϵ when its value is sufficiently small. The insets in (b, d) show the nonlinear correction to the break-up time $\Delta t_{\rm NL}$ as a function of β.

by these authors by means of the thread radius at $z = 0$ close to pinch-off, instead of using either V_{sat} or R_{sat}.

Figures 7(a,b) show the discontinuous transition in $V_{\rm sat}$ and $\Sigma_{\rm sat}$ that occurs when β is increased above the critical value $\beta_c(La = 0.01) = 0.978 \pm 0.0003$. For $\beta > \beta_c(La = 0.01)$ a satellite drop centered at $z = 0$ is formed, trapping approximately 2.1% of the total volume of liquid and 4.5% of the total mass of surfactant.

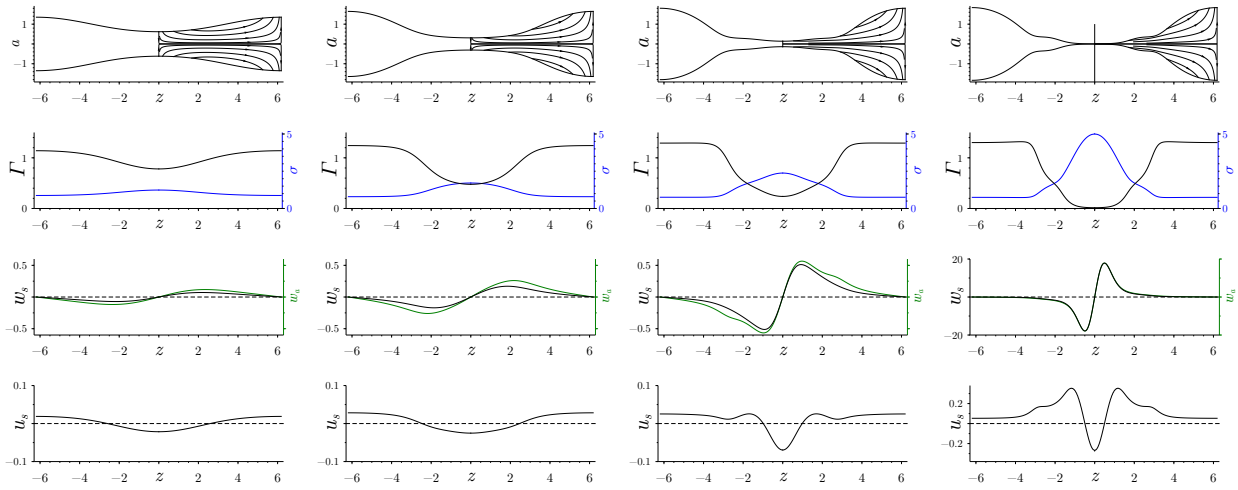

(a) $t = 100$ (b) $t = 112$ (c) $t = 118$ (d) $t = 119.02$

Figure 8: Temporal evolution of the liquid thread radius a (first row), surfactant concentration Γ (second row, black lines), surface tension σ (second row, blue lines), axial velocity at the interface w_s (third row, black lines) and at the centreline w_a (third row, green lines), and radial surface velocity u_s (fourth row), for $La = 0.01$, $\epsilon = 10^{-3}$ and $\beta = 0.960 < \beta_c(La = 0.01)$, with $k = k_m = 0.508$. The vertical line in the last snapshot of a indicates the position of $z_{\min}$.

3.3.3. *Physical explanation of the discontinuous transition*

To explain the abrupt transition induced by the presence of surfactants, figures 8 and 9 show the temporal evolution of the liquid thread for $La = 0.01$ and two different values of β, namely $\beta = 0.960 < \beta_c(La = 0.01)$, with $k = k_m = 0.508$, and $\beta = 0.979 > \beta_c(La = 0.01)$, with $k = k_m = 0.512$, respectively. In both cases, we have computed the thread radius a (first row), the surfactant concentration Γ together with the surface tension σ (second row), the axial velocity at the interface, w_s, and at the centreline, w_a (third row), and the radial surface velocity u_s (fourth row). Time is indicated in the labels.

The presence of surfactants introduces two main effects. The advection of surfactant molecules outside the central region of the thread increases the local surface tension in this region, as can be observed in the figures 8(a) and 9(a). This surfactant depletion generates two opposed effects: first, the axial capillary pressure gradient is enhanced, since the value of σ becomes larger in the central region, where Γ is smaller, while σ becomes smaller away from the center, where Γ is larger. Second, there is a stabilising effect induced by the elastic or Marangoni stress, which competes with the destabilising Plateau-Rayleigh mechanism enhanced by the first effect. Actually, the gradient of σ generates a tangential stress at the interface directed towards increasing values of σ, which opposes the drainage flow and tends to replenish the central zone with surfactant.

In the case of $\beta < \beta_c(La = 0.01)$, figure 8($b$,$c$) shows that the Marangoni stress reduces the axial surface velocity, w_s, compared with the centreline velocity, w_a, the difference between both velocities being larger in the region where $\boldsymbol{\nabla}_s\sigma$ is higher. As the fluid is drained from the center for increasing times, $\boldsymbol{\nabla}_s\sigma$ becomes larger. When $\beta < \beta_c(La = 0.01)$ the capillary pressure gradient is able to remove the whole fluid from the center, where the liquid thread finally detaches, as evidenced by figure 8(d). Note

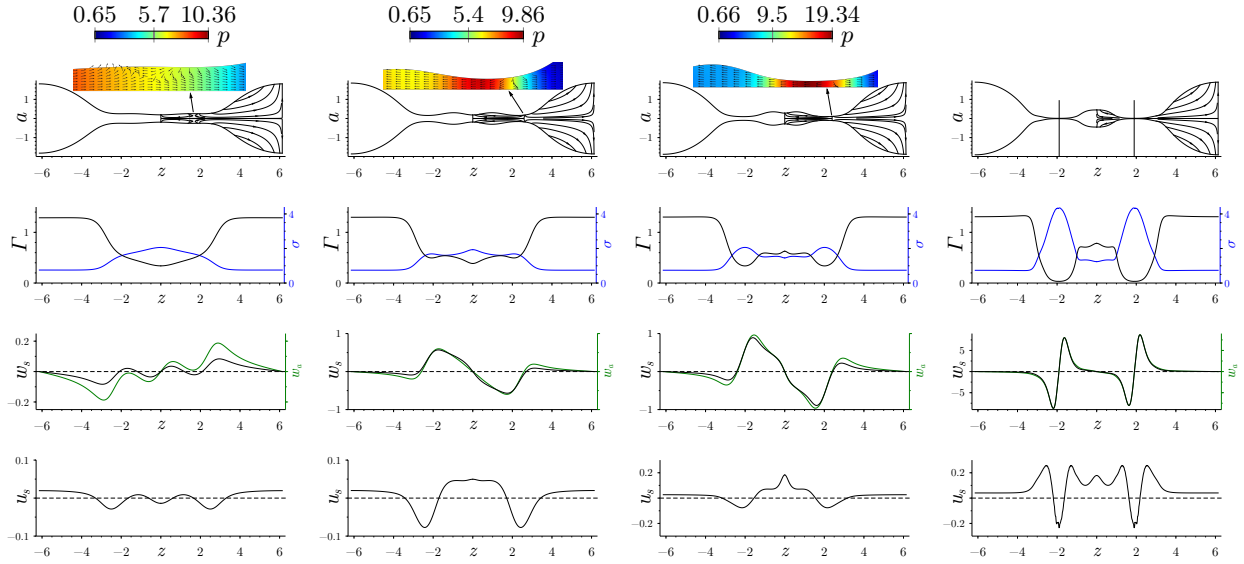

(*a*) $t = 119.8$ (*b*) $t = 122$ (*c*) $t = 122.8$ (*d*) $t = 123.71$

Figure 9: Same as figure 8 but for $\beta = 0.979 > \beta_c(La = 0.01)$, with $k = k_m = 0.512$. The insets are zooms showing the normalised velocity vector field and isocontours of the pressure field.

that, during the thread evolution, two bulges connecting the central and outer regions grow due to the reduction of the surface velocity, and are finally connected by a thin liquid thread close to pinch-off.

When $\beta > \beta_c(La = 0.01)$ the foregoing explanation still holds, but the elastic stress is large enough to revert the flow near the interface, as shown in figure 9(*a*). The associated stagnation point diffuses radially inwards, and leads to a counterflow separating a region where liquid flows towards the center and induces the formation of a satellite, from another region where the incipient main drop is fed with liquid. Consequently, the thread detaches in between these two regions. If β increases further, the break-up time increases and the flow reversal occurs at earlier stages, so that $V_{\rm sat}$ and $\Sigma_{\rm sat}$ increase monotonically, as shown in figures 7(*a*,*b*).

When $La = 100$, figures 7(*c*,*d*) show that the effect of surface elasticity is much weaker in the case of dominant inertia, as was anticipated both in figure 5 and also by the shapes shown in the upper row of figure 4. The small influence of insoluble surfactants in the inviscid limit, $La \gg 1$, had been already noted in the linear stability analyses of Whitaker (1976), Hansen *et al.* (1999) and Timmermans & Lister (2002). Indeed, the effect of Marangoni stresses is confined to a thin boundary layer at the free surface, where the viscous stress rapidly restores any imbalance of σ, and which does not have any influence in the bulk liquid motion. Consequently, for $La = 100$, the satellite volume, $V_{\rm sat}$, varies only slightly with respect to the value of a clean liquid thread, $V_{\rm sat}(\beta = 0, La = 100) \simeq 0.03$, with a minimum at $\beta \simeq 0.203$, whereas $\Sigma_{\rm sat}$ increases monotonically as β increases. To explain this result, figures 10 and 11 show two sets of snapshots of a, Γ, σ, w_s, w_a and u_s for $\beta = 0.203$, at which $V_{\rm sat}$ is minimum, and for $\beta = 1$, respectively.

In the weak-elastic limit, $\beta \to 0$, a satellite droplet with volume $V_{\rm sat} \simeq 3\%$ is formed at pinch-off, as already shown in figures 5 and 7(*c*). The satellite volume decreases as β increases in the range $0 < \beta \lesssim 0.203$. Indeed, when β increases, the Marangoni

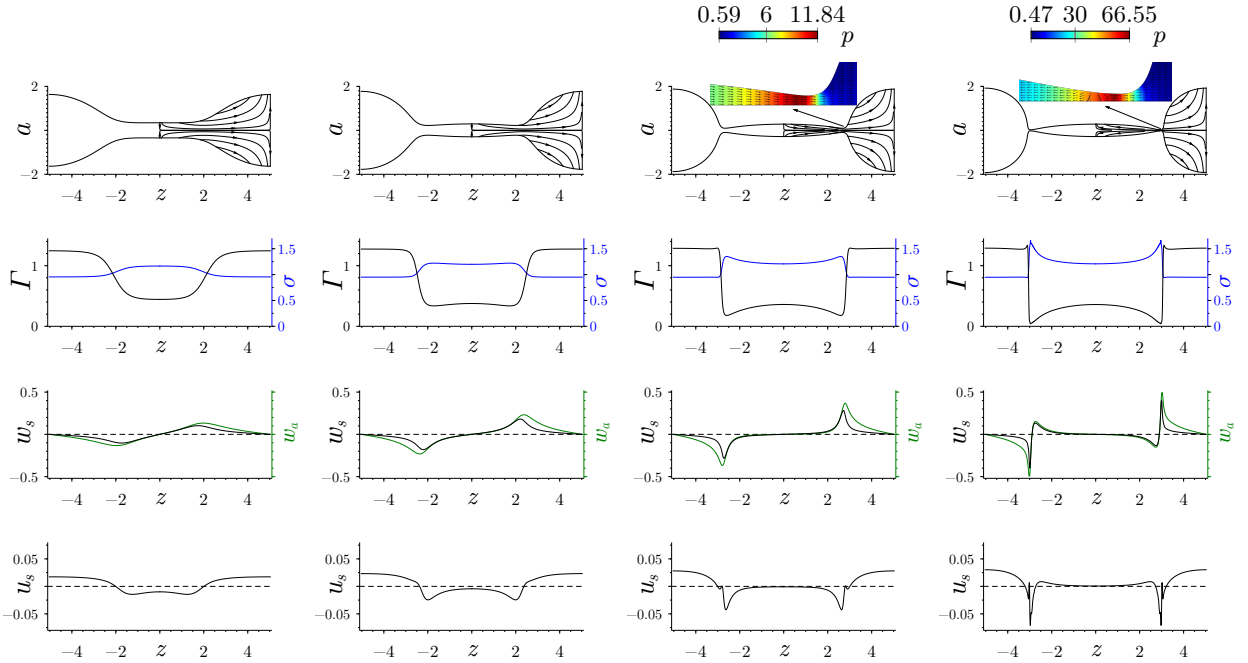

(a) $t = 269$ (b) $t = 276$ (c) $t = 280$ (d) $t = 281.55$

Figure 10: Same as figure 8 but for $La = 100$ and $\beta = 0.203$, with $k = k_m = 0.625$.

rigidification of the interface slows down the pinch-off process by decreasing the interfacial velocities, as evidenced by the time evolution of w_s, w_a and u_s in figure 10 with respect to figure 6(*e–h*). The latter behaviour, together with the fact that the pressure gradient is locally enhanced due to the variations of σ, explain why a larger volume is drained from the satellite droplet compared with the case of a clean interface. However, the Marangoni stress that opposes the drainage flow away from the center reduces the advection of surfactant towards the main drops, and thus the value of Σ_{sat} increases, as shown in figure 7(*d*). The snapshot in figure 10(*d*) shows that only very close to break-up the flow is reversed near the neck region, although without overturning of the main drop. This behaviour at high values of La and low values of β was previously noticed by Kamat *et al.* (2018), who showed that the stagnation point occurs at earlier stages in surfactant-laden interfaces compared with clean interfaces, due to the strong Marangoni stress in the neck region.

A representative case of $La = 100$ and $\beta > 0.203$ is shown in the snapshots of figure 11 for $\beta = 1$. The main change with respect to the preceding case is the fact that for $\beta = 1$ the Marangoni stress is strong enough to revert the surface flow at earlier stages, as shown in panels (*b*) and (*d*). Therefore, the stagnation point appears earlier than in the case of figure 10, and diffuses almost instantaneously in the radial direction, leading to a satellite droplet with larger values of the normalised volume and of the surfactant mass. It can thus be deduced that the minimum value of V_{sat} displayed in figure 7(*c*) appears due to a competition between the two aforementioned opposite effects induced by the presence of surfactant.

For an intermediate value of La within the range $0.049 < La < 7.5$, the two effects described previously coexist when β is increased, as shown by the isocontours of V_{sat}

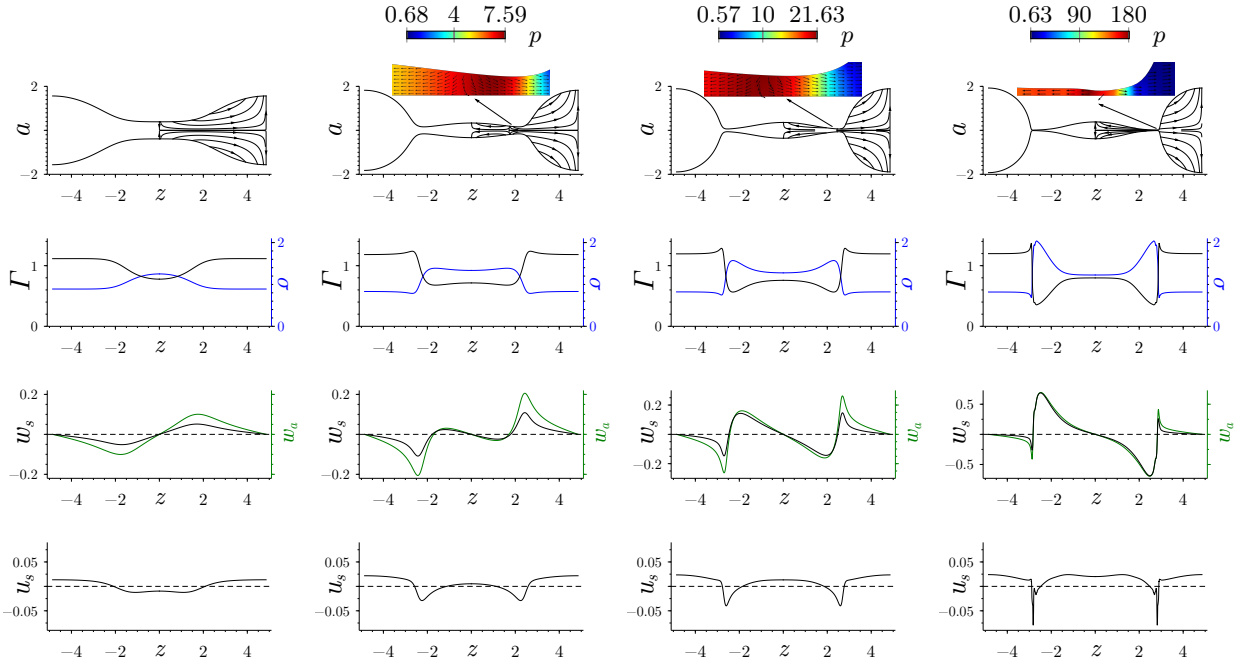

(*a*) $t = 290$ (*b*) $t = 305$ (*c*) $t = 308$ (*d*) $t = 309.42$

Figure 11: Same as figure 10 but for $\beta = 1$ with $k = k_m = 0.647$.

in figure 5. For instance, when $La = 1$, $V_{\rm sat}$ first decreases as β increases, and when the elastic stress is strong enough, the flow is reversed and the discontinuous transition occurs. Note that, in the latter case, inertia is important since La is of order unity, and a small but finite satellite droplet exists in the clean limit, $\beta \to 0$ (see e.g. the second row of figure 4). Hence, the main difference with respect to the limit $La \gg 1$ is that in this case, since $V_{\rm sat}(\beta \to 0)$ is small, the increase of β reduces the satellite volume and may even make it negligible. The latter effect happens when $0.049 < La < 1.69$, where $V_{\rm sat}$ is reduced below our numerical cut-off at some point when $\beta < \beta_c$ (see figures 3 and 5). Within the range $1.69 < La < 7.5$, $V_{\rm sat}$ does not become negligible when $\beta < \beta_c(La)$. Besides, in the whole range $0.049 < La < 7.5$, $\Sigma_{\rm sat}$ also decreases monotonically together with $V_{\rm sat}$ when $\beta < \beta_c$, what can be explained by the fact that $V_{\rm sat}$ is small when $\beta = 0$, so that $\Sigma_{\rm sat}$ necessarily decreases when β is increased.

Let us recall at this point that the critical elasticity, $\beta_c(La)$, decreases as La increases within the range $0 < La < 7.5$, as shown in figures 3 and 5. The reason for the latter trend is the fact that the advection of surfactant away from the central region is enhanced by the liquid inertia, so that $\boldsymbol{\nabla}_s\sigma$ also increases, and thus the value of β for which the elastic stress reverts the flow is smaller. For larger values of La, the value of $V_{\rm sat}(La, \beta \to 0)$ increases, and therefore the jumps experienced by $V_{\rm sat}$ and $\Sigma_{\rm sat}$ at the discontinuous transition, $\beta = \beta_c$, decrease. Finally, for $La > 7.5$, the discontinuous transition disappears.

3.3.4. *Scaling laws for V_{sat} and Σ_{sat} as functions of La*

Figure 12 shows $V_{\rm sat}$ and $\Sigma_{\rm sat}$ as functions of La for different values of β indicated in the legend. The circle with error bars corresponds to the experiment of Rutland & Jameson (1971) on the natural break-up of a liquid jet of clean water, which is in close agreement

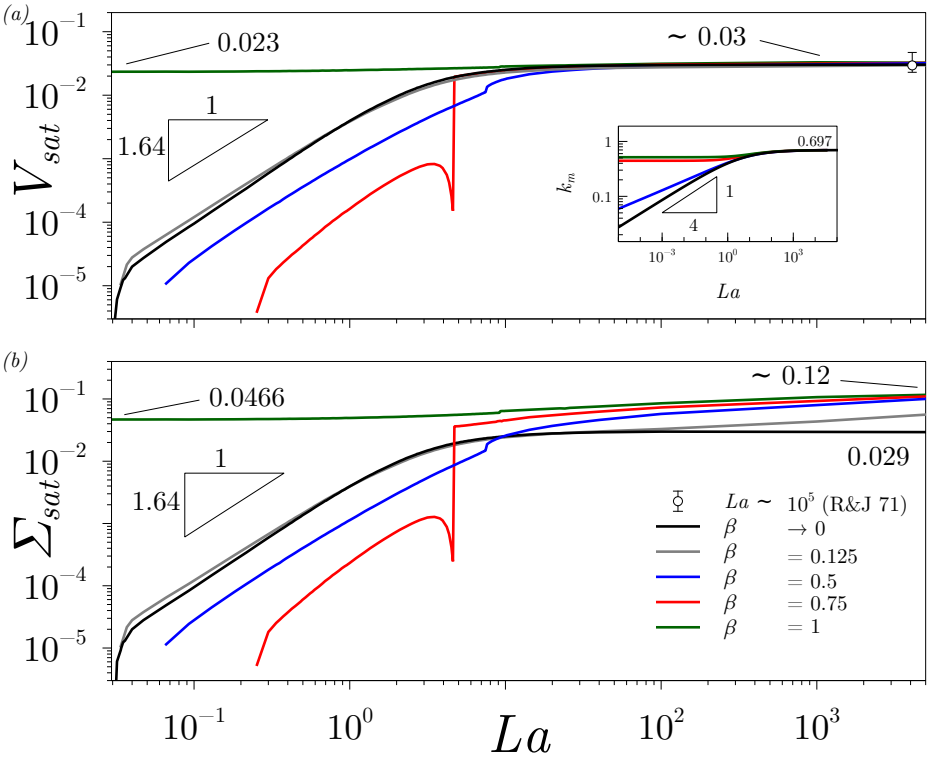

Figure 12: Normalised satellite's volume V_{sat}, and normalised mass of surfactant trapped at its interface $\Sigma_{\rm sat}$, as a function of the Laplace number La in log-log for different values of β indicated in the legend. The inset shows the dependence of the maximum amplification wavenumber k_m with respect to La in log-log. The circle with error bars corresponds to the experiments of the natural break-up of a liquid jet of water performed by Rutland & Jameson (1970).

with our numerical result for $\beta = 0$. The inset displays the most unstable wavenumber, k_m, as a function of La, showing the inviscid plateau $k_m \simeq 0.697$ for $La \gg 1$ (Rayleigh 1878), as well as the power-law dependence for small values of La. The latter power law can be deduced from the long-wave approximation of the dispersion relation (3.2) or, equivalently, from the leading-order one-dimensional (1D) model deduced by Eggers & Dupont (1994) and García & Castellanos (1994). In the clean case, $\beta = 0$, the leading-order 1D result is $k_m \sim [2 + 3\sqrt{2}La^{-1/2}]^{-1/2}$ and $\omega_m \sim [2\sqrt{2} + 6La^{-1/2}]^{-1}$ (Eggers & Villermaux 2008). The latter long-wave result provides very accurate results in the whole range of La, since $k \in (0, 1)$ accomplishes the slenderness assumption. In the inviscid limit, $La \to \infty$, both ω_m and k_m are slightly overestimated by the 1D model, namely $\omega_m \to 2^{-3/2}$ and $k_m \to 2^{-1/2}$. However, in the Stokes limit, $La \ll 1$, the values of $\omega_m \to 1/6$ and $k_m = 3^{-1/2}2^{-1/4}La^{1/4}$ are in excellent agreement with the exact linear theory. When $\beta > 1/2$, the elastic stress regularises k_m in the limit of $La \to 0$, as analysed in detail by Timmermans & Lister (2002) (see also the isocontours of k_m in figure 3 *c*).

In the limit of a clean interface, $\beta = 0$, $V_{\rm sat}$ increases monotonically with La, as previously explained in figure 6. In particular, our numerical results have revealed that the satellite volume scales as $V_{\rm sat} = 0.00421La^{1.64}$ within a range of almost two decades in La, namely $0.05 \lesssim La \lesssim 2$. Alternatively, using the expression for the equivalent

radius $R_{\rm sat}$ developed in §3.2, which depends on k_m, and since $k_m = 3^{-1/2}2^{-1/4}La^{1/4}$ within the range of La for which $V_{\rm sat}$ exhibits power-law scaling, it is deduced that $R_{\rm sat} = 0.34La^{0.463}$. When $La \lesssim 0.05$ the value of $V_{\rm sat}$ exhibits a very fast decrease and rapidly becomes negligibly small, corresponding to the regime where the main droplets are connected with ultrathin threads. In the opposite limit, namely for $La \gtrsim 10$, the value of $V_{\rm sat}$ reaches a plateau of about 3%, as already discussed in the context of figures 5 and 7(c). Equivalently, since $k_m \simeq 0.697$ when $La \gg 1$, $R_{\rm sat} \simeq 0.588$ in the inviscid limit, in excellent agreement with the experiments of Rutland & Jameson (1971) (circle with error bars in figure 12a), and also with the numerical simulations of Ashgriz & Mashayek (1995). In the weak-elasticity limit, $\beta < 0.125$, the behaviour of $\Sigma_{\rm sat}$ is identical to that of $V_{\rm sat}$, displaying the same scaling law within the same range in La, and also reaching an inviscid plateau of about 2.9% when $La \gtrsim 10$.

Figure 12 also shows that, when $La \gg 1$, the 3% plateau reached by $V_{\rm sat}$ is barely affected by β since, as explained previously, inertia dominates and the elastic stress cannot induce any substantial change in the bulk motion (Whitaker 1976; Hansen *et al.* 1999; Timmermans & Lister 2002). As inertia increases, the dependence of $V_{\rm sat}$ on β becomes even weaker than in the case of $La = 100$ displayed in figure 7(c). Although the satellite shape at pinch-off is the same, $\Sigma_{\rm sat}$ reaches different inviscid limits as β increases. In particular, the 2.9% inviscid plateau reached by $\Sigma_{\rm sat}$ in the weak-elasticity limit increases with β, the reason being the same as in the case of figure 7(d).

When $\beta = 1 > \beta_c(La)\ \forall\ La$, a satellite is always formed for any value of La, and both $V_{\rm sat}$ and $\Sigma_{\rm sat}$ increase smoothly with La as inertia becomes more important. In fact, $V_{\rm sat}$ and $\Sigma_{\rm sat}$ reach respective plateaus both in the Stokes and Euler limits. For $La \to 0$, the values of $V_{\rm sat}$ and $\Sigma_{\rm sat}$ are about 2.30% and 4.67%, respectively, whereas in the limit $La \to \infty$, their values are 3% and 12%, approximately. This trend prevails provided that $\beta > \beta_c(La \to 0) = 0.978$, as shown in the isocontours of $V_{\rm sat}$ and $\Sigma_{\rm sat}$ in figure 5. Hence, in the elasticity-dominated regime where $\beta > \beta_c$, the effect of inertia on $V_{\rm sat}$ and $\Sigma_{\rm sat}$ is weaker, although the column for $\beta = 1$ in figure 4 reveals that the shape of the thread at pinch-off changes substantially. As already mentioned, inertia tends to form oval-shaped satellites, which are more likely to break-up in the relaxation process after pinch-off, whereas the surface elasticity tends to form spherical satellites which will not experience secondary break-up events.

4. Conclusions

In this paper we have reported an exhasutive numerical study of the unforced break-up of free axisymmetric threads of Newtonian liquid whose interface is coated with insoluble surfactants. Our main objective was to describe and explain how the presence of these molecules affects the nonlinear dynamics of the liquid thread and the satellite drop formation regimes when the dynamics is triggered by the most dangerous initial disturbance. Under these conditions we have shown that, when the initial perturbation amplitude is sufficiently small, the flow depends on two dimensionless parameters, namely the Laplace number La and the elasticity parameter β. Our numerical simulations have allowed us to characterise the influence of these two parameters on the satellite volume $V_{\rm sat}$, the mass of surfactant trapped at its interface $\Sigma_{\rm sat}$, the nonlinear correction to the linear break-up time $\Delta t_{\rm NL}$, and the satellite sphericity $\mathcal{S}$, all of them computed at times very close to break-up. Using these measures, we have shown that the (La, β) parameter plane presents two distinguished regions: a region without satellite formation takes place for small enough values of La and β, while satellite droplets are formed in the remaining parameter plane. It is important to emphasise that our numerical simulations do not

contemplate the post break-up behaviour of the threads and satellites, including their relaxation or eventual secondary break-up events. Indeed, an accurate analysis of the dynamics beyond break-up is an important though technically challenging task, that is out of the scope of the present study. Clearly, a future task to be pursued is to extend the present results by performing numerical simulations that are able to compute the post pinch-off dynamics to unveil the ultimate state of the unstable liquid thread.

We have found a discontinuous transition at a critical elasticity number $\beta = \beta_c(La)$ within the range $0 < La < 7.5$, and at which $V_{\rm sat}$ and $\Sigma_{\rm sat}$ change abruptly. We have explained this behaviour in terms of a competition between the Plateau-Rayleigh instability mechanism and the elastic or Marangoni stresses that arise due to interfacial surface tension gradients. When β is high enough, the elastic stress that opposes the flow induced by the capillary pressure gradient is able to revert it at the interface. Afterwards, the surface stagnation point diffuses radially inwards, and finally a net flux of liquid swells the central region forming a satellite droplet prior to pinch-off.

When $1.69 < La < 7.5$, $V_{\rm sat}$ and $\Sigma_{\rm sat}$ increase from a non-zero satellite droplet for $\beta < \beta_c$, to a larger value when $\beta > \beta_c$. For $La < 1.69$ the abrupt transition always occurs from a negligible satellite droplet as β surpasses β_c. When $La \lesssim 0.2$, the critical elasticity number reaches a plateau, $\beta_c = 0.978$, for $La = 7.5$ $\beta_c = 0.546$, and finally when $La > 7.5$ the abrupt transition disappears. In between, β_c decreases monotonically with La, since inertia enhances the gradients of surface tension.

For a clean liquid thread, $\beta \to 0$, we have provided a new scaling law for the normalised satellite volume, namely $V_{\rm sat} = 0.00421 La^{1.64}$, which is valid in the range $0.05 \lesssim La \lesssim 1$. We have shown the existence of a regular weak-elasticity limit, $\beta < 0.125$, for which the latter scaling law holds, and for which the normalised mass of surfactant carried by the satellite, $\Sigma_{\rm sat}$, exhibits the same scaling law as $V_{\rm sat}$. In this limit, when inertia is sufficiently dominant, namely $La \gtrsim 10$, both $V_{\rm sat}$ and $\Sigma_{\rm sat}$ reach respective limits of about 3% and 2.9%, the value of 3% being in close agreement with previous experiments (Rutland & Jameson 1971) and numerical simulations (Ashgriz & Mashayek 1995). In contrast, for any value of β, when $La \ll 1$ both $V_{\rm sat}$ and $\Sigma_{\rm sat}$ become negligible. The value of La at which the latter behaviour takes place depends on β.

The 3% inviscid plateau in $V_{\rm sat}$ varies slightly with β, and displays a minimum within the range $0.2 \lesssim \beta \lesssim 0.4$, whereas the 2.9% inviscid plateau of $\Sigma_{\rm sat}$ increases monotonically. The existence of this minimum has been explained by the competition between two opposed effects induced by the presence of surfactants: (I) the reduction of the surface tension σ when Γ increases, which enhances the capillary pressure gradient, and (II) the Marangoni stress exerted at the interface due to the gradients of σ. The initial decrease of $V_{\rm sat}$ when β grows is due to (I), whereas the increase above the minimum value is due to (II), which is able to revert the flow at earlier stages of the thread evolution when β is sufficiently high. The decrease of $V_{\rm sat}$ with β also coexists with the abrupt transition in the range $0.049 \lesssim La < 7.5$. Additionally, the increase of $\Sigma_{\rm sat}$ when $La > 7.5$ is explained by the reduction of the interfacial velocity due to (II), what tends to accumulate surfactant molecules at the satellite.

When $La \gg 1$, the effect of surface elasticity is very weak, since its effect is confined to a thin Marangoni boundary layer at the interface, where viscous dissipation tends to restore a modified but constant value of σ. The most important effect of β in the inviscid limit is the fact that $\Sigma_{\rm sat}$ increases with β due to the reason explained in the previous paragraph.

Here, we have considered a nonlinear equation of state for $\sigma(\Gamma)$ that is deduced from the equilibrium thermodynamics of the interface together with the conservation of molecules in the insoluble limit. We have shown that using this nonlinear equation

leads to substantial quantitative differences with respect to the use of its linearised version (Dravid *et al.* 2006). These differences call out for a careful experimental study of the present jet flow configuration or a similar one, e.g. a cylindrical liquid bridge between two static disks whose length is above the critical one for spontaneous break-up. The latter configuration has been recently studied experimentally by Kovalchuk *et al.* (2018) for concentrations above the CMC. An experimental campaign would also be needed to probe the validity of the insoluble approximation. In fact, it would be interesting to extend the present numerical study to the soluble case, contemplating both bulk diffusion and sorption kinetics.

Another feature that deserves future work is the effect of surface diffusion on the satellite drop formation regimes described herein, especially in cases where $La \lesssim O(1)$, for which the surface diffusion time could be of the order of the thread break-up time. Similarly, for small-scale threads, the surface shear and dilational viscosities could also play an important role (Boussinesq 1913; Scriven 1960; Martínez-Calvo & Sevilla 2018). The present numerical analysis should also be extended together with the experiments, to unveil the conditions under which diffusive and surface viscous effects become relevant, and how they affect the transitions described in the present work.

Acknowledgements

A.M.-C. and A.S. thank the Spanish MINECO, Subdirección General de Gestión de Ayudas a la Investigación, for its support through projects DPI2014-59292-C3-1-P and DPI2015-71901-REDT, and the Spanish MCIU-Agencia Estatal de Investigación through project DPI2017-88201-C3-3-R. These research projects have been partly financed through FEDER European funds. A.M.-C. also acknowledges support from the Spanish MECD through the grant FPU16/02562, and to its associated program Ayudas a la Movilidad 2017 during his stay at TIPs–ULB, Brussels. J.R.-R. and B.S. thank the F.R.S.-FNRS for financial support.

REFERENCES

Ambravaneswaran, B. & Basaran, O.A. 1999 Effects of insoluble surfactants on the nonlinear deformation and breakup of stretching liquid bridges. *Phys. Fluids* **11** (5), 997–1015.

Ambravaneswaran, B., Subramani, H.J., Phillips, S.D. & Basaran, O.A. 2004 Dripping-jetting transitions in a dripping faucet. *Phys. Rev. Lett.* **93**, 034501.

Anna, S.L. 2016 Droplets and bubbles in microfluidic devices. *Annu. Rev. Fluid Mech.* **48**, 285–309.

Ashgriz, N. & Mashayek, F. 1995 Temporal analysis of capillary jet breakup. *J. Fluid Mech.* **291**, 163–190.

Bogy, D.B. 1979 Drop formation in a circular liquid jet. *Annu. Rev. Fluid Mech.* **11**, 207–228.

Boussinesq, J.V. 1913 *J. Ann. Chim. Phys.* **29**, 349.

Campana, D.M. & Saita, F.A. 2006 Numerical analysis of the rayleigh instability in capillary tubes: The influence of surfactant solubility. *Phys. Fluids* **18**, 022104.

Champougny, L., Scheid, B., Restagno, F., Vermant, J. & Rio, E. 2015 Surfactant-induced rigidity of interfaces: a unified approach to free and dip-coated films. *Soft Matter* **11** (14), 2758–2770.

Chandrasekhar, S. 1961 *Hydrodynamic and Hydromagnetic Stability*. ed and Transl. E MacCurdy (New York: George Brazillier).

Chaudhary, K.C. & Maxworthy, T. 1980 The nonlinear capillary instability of a liquid jet. part 3. experiments on satellite drop formation and control. *J. Fluid. Mech.* **96** (2), 287–297.

Christopher, G.F. & Anna, S.L. 2007 Microfluidic methods for generating continuous droplet streams. *J. Phys. D: Appl. Phys.* **40**, R319–R336.

Craster, R.V., Matar, O.K. & Papageorgiou, D.T. 2002 Pinchoff and satellite formation in surfactant covered viscous threads. *Phys. Fluids* **14** (4), 1364–1376.

Craster, R.V., Matar, O.K. & Papageorgiou, D.T. 2009 Breakup of surfactant-laden jets above the critical micelle concentration. *J. Fluid Mech.* **629**, 195–219.

Delacotte, J., Montel, L., Restagno, F., Scheid, B., Dollet, B., Stone, H.A., Langevin, D. & Rio, E. 2012 Plate coating: influence of concentrated surfactants on the film thickness. *Langmuir* **28** (8), 3821–3830.

Derby, B. 2010 Inkjet printing of functional and structural materials: Fluid property requirements, feature stability, and resolution. *Annu. Rev. Mater. Res.* **40**, 395–414.

Donnelly, R.J. & Glaberson, W.I. 1966 Experiments on the capillary instability of a liquid jet. *Proc. Roy. Soc.* **A290**, 547–566.

Dravid, V., Songsermpong, S., Xue, Z., Corvalan, C.M. & Sojka, P.E. 2006 Two-dimensional modeling of the effects of insoluble surfactant on the breakup of a liquid filament. *Chem. Eng. Sci.* **61**, 3577–3585.

Eggers, J. 1993 Universal pinching of 3d axisymmetric free-surface flow. *Phys. Rev. Lett.* **71**, 3458.

Eggers, J 1997 Nonlinear dynamics and breakup of free surface flows. *Rev. Mod. Phys.* **69**, 865–929.

Eggers, J. & Dupont, T.F. 1994 Drop formation in a one-dimensional approximation of the Navier-Stokes equation. *J. Fluid Mech.* **262**, 205–222.

Eggers, J. & Villermaux, E. 2008 Physics of liquid jets. *Rep. Prog. Phys.* **71**, 036601.

García, F.J. & Castellanos, A. 1994 One-dimensional models for slender axisymmetric viscous liquid jets. *Phys. Fluids* **6** (8), 2676–2689.

Goedde, E.F. & Yuen, M.C. 1970 Experiments on liquid jet instability. *J. Fluid Mech.* **40** (3), 495–511.

González, H. & García, F.J. 2009 The measurement of growth rates in capillary jets. *J. Fluid Mech.* **619**, 179–212.

Hansen, S., Peters, G.W.M. & Meijer, H.E.H. 1999 The effect of surfactant on the stability of a fluid filament embedded in a viscous fluid. *J. Fluid Mech.* **382**, 331–349.

Kalaaji, A., Lopez, B., Attane, P. & Soucemarianadin, A. 2003 Breakup length of forced liquid jets. *Phys. Fluids* **15**, 2469–2479.

Kamat, P.M., Wagoner, B.W., Thete, S.S. & Basaran, O.A. 2018 Role of marangoni stress during breakup of surfactant-covered liquid threads: Reduced rates of thinning and microthread cascades. *Phys. Rev. Fluids* **3** (4), 043602.

Keller, J.B., Rubinow, S.I. & Tu, Y.O. 1973 Spatial instability of a jet. *Phys. Fluids* **16**, 2052–2055.

Kovalchuk, N. M., Jenkinson, H., Miller, R. & Simmons, M. J. H. 2018 Effect of soluble surfactants on pinch-off of moderately viscous drops and satellite size. *J. Colloid Interf. Sci.* **516**, 182–191.

Kowalewski, T. A 1996 On the separation of droplets from a liquid jet. *Fluid Dyn. Res.* **17**, 121–145.

Lafrance, P. 1975 Nonlinear breakup of a laminar liquid jet. *Phys. Fluids* **18** (4), 428–432.

Langevin, D. 2014 Rheology of adsorbed surfactant monolayers at fluid surfaces. *Annu. Rev. Fluid Mech.* **46**, 47–65.

Lee, H.C. 1974 Drop formation in a liquid jet. *IBM Journal of Research and Development* **18** (4), 364–369.

Leib, S.J. & Goldstein, M.E. 1986*a* Convective and absolute instability of a viscous liquid jet. *Phys. Fluids* **29** (4), 952–954.

Leib, S.J. & Goldstein, M.E. 1986*b* The generation of capillary instabilities on a liquid jet. *J. Fluid Mech.* **168**, 479–500.

Liao, Y.C., Franses, E.I. & Basaran, O.A. 2006 Deformation and breakup of a stretching liquid bridge covered with an insoluble surfactant monolayer. *Phys. Fluids* **18** (2), 022101.

Magnus, G. 1859 *Ann. Phys. Chem.* **106**, 1.

Mansour, Nagi N & Lundgren, Thomas S 1990 Satellite formation in capillary jet breakup. *Phys. Fluids A: Fluid Dyn.* **2** (7), 1141–1144.

Martínez-Calvo, A., Rubio-Rubio, M. & Sevilla, A. 2018 The nonlinear states of viscous capillary jets confined in the axial direction. *J. Fluid Mech.* **834**, 335–358.

Martínez-Calvo, A. & Sevilla, A. 2018 Temporal stability of free liquid threads with surface viscoelasticity. *J. Fluid Mech.* **846**, 877–901.

Mashayek, F. & Ashgriz, N. 1995 Nonlinear instability of liquid jets with thermocapillarity. *J. Fluid Mech.* **283**, 97–123.

McGough, P.T. & Basaran, O.A. 2006 Repeated formation of fluid threads in breakup of a surfactant-covered jet. *Phys. Rev. Lett.* **96** (5), 054502.

Papageorgiou, D.T. 1995 On the breakup of viscous liquid threads. *Phys. Fluids* **7** (7), 1529–1544.

Pereira, A. & Kalliadasis, S. 2008 On the transport equation for an interfacial quantity. *Eur. Phys. J. Appl. Phys.* **44** (2), 211–214.

Plateau, J. 1873 *Statique expérimentale et théorique des liquides*. Gauthier-Villars et C^{ie}, Paris.

Ponce-Torres, A., Montanero, J.M., Herrada, M.A., Vega, E.J. & Vega, J.M. 2017 Influence of the surface viscosity on the breakup of a surfactant-laden drop. *Phys. Rev. Lett.* **118**, 024501.

Rayleigh, W.S. 1878 On the instability of jets. *Proc. R. Soc. Lond.* **10**, 4–13.

Rayleigh, W.S. 1882 Further observations upon liquid jets, in continuation of those recorded in the royal society's 'proceedings' for march and may. *Proc. R. Soc. Lond.* pp. 130–145.

Rayleigh, W.S. 1892 On the instability of a cylinder of viscous liquid under capillary force. *Phil. Mag. and J. Science* .

Rivero-Rodríguez, J. & Scheid, B. 2018*a* Bubble dynamics in microchannels: inertial and capillary migration forces. *J. Fluid Mech.* **842**, 215–247.

Rivero-Rodríguez, J. & Scheid, B. 2018*b* Bubble dynamics in microchannels: inertial and capillary migration forces – CORRIGENDUM. *J. Fluid Mech.* **855**, 1242–1245.

Roché, M., Aytouna, M., Bonn, D. & Kellay, H. 2009 Effect of surface tension variations on the pinch-off behavior of small fluid drops in the presence of surfactants. *Phys. Rev. Lett* **103** (26), 264501.

Rubio-Rubio, M., Sevilla, A. & Gordillo, J.M. 2013 On the thinnest steady threads obtained by gravitational stretching of capillary jets. *J. Fluid Mech.* **729**, 471–483.

Rutland, D.F. & Jameson, G.J. 1970 Theoretical prediction of the sizes of drops formed in the breakup of capillary jets. *Chem. Eng. Sci.* **25** (11), 1689–1698.

Rutland, D.F. & Jameson, G.J. 1971 A non-linear effect in the capillary instability of liquid jets. *J. Fluid Mech.* **46** (2), 267–271.

Savart, F. 1833 Mémoire sur la constitution des veines liquides lancées par des orifices circulaires en mince paroi. *Ann. Chim.* **53**, 337–386.

Scheid, B., Delacotte, J., Dollet, B., Rio, E., Restagno, F., van Nierop, E.A., Cantat, I., Langevin, D. & Stone, H.A. 2010 The role of surface rheology on liquid film formation. *EPL* **90**, 24002.

Scriven, L.E. 1960 Dynamics of a fluid interface. Equation of motion for Newtonian surface fluids. *Chem. Eng. Sci.* **12** (2), 98–108.

Siderius, A., Kehl, S. K. & Leaist, D. G. 2002 Surfactant diffusion near critical micelle concentrations. *J. Solution Chem.* **31** (8), 607–625.

Stone, H.A. 1990 A simple derivation of the time-dependent convective-diffusion equation for surfactant transport along a deforming interface. *Phys. Fluids A* **2** (1), 111–112.

Subramani, H.J., Yeoh, H.K., Suryo, R., Xu, Q., Ambravaneswaran, B. & Basaran, O.A. 2006 Simplicity and complexity in a dripping faucet. *Phys. Fluids* **18** (3), 032106.

Timmermans, M.-L. & Lister, J.R. 2002 The effect of surfactant on the stability of a liquid thread. *J. Fluid Mech.* **459**, 289–306.

Whitaker, S. 1976 Studies of the drop-weight method for surfactant solutions III. Drop stability, the effect of surfactants on the stability of a column of liquid. *J. Colloid Interf. Sci.* **54** (2), 231–248.

Wong, H., Rumschitzki, D. & Maldarelli, C. 1996 On the surfactant mass balance at a deforming fluid interface. *Phys. Fluids* **8** (11), 3203–3204.

Xu, Q., Liao, Y.-C. & Basaran, O.A. 2007 Can surfactant be present at pinch-off of a liquid filament? *Phys. Rev. Lett.* **98** (5), 054503.

Yildirim, O. E., Xu, Q. & Basaran, O. A. 2005 Analysis of the drop weight method. *Phys. Fluids* **17**, 062107.

Yuen, M.-C. 1968 Non-linear capillary instability of a liquid jet. *J. Fluid Mech.* **33** (1), 151–163.